SIMULATION OF SECONDARY FLOWS IN NEWTONIAN AND VISCOELASTIC FLUIDS THROUGH VARIOUS SHAPED CONDUITS

TUPTHAI SEETHAO

A THESIS SUBMITTED IN PARTIAL FULFILLMENT

OF THE REQUIREMENTS FOR THE DEGREE OF

MASTER OF ENGINEERING IN CHEMICAL ENGINEERING

FACULTY OF ENGINEERING

KING MONGKUT'S INSTITUTE OF TECHNOLOGY LADKRABANG

2014

KMITL-2014-EN-M-220-145

หัวข้อวิทยานิพนธ์	การจำลองของการไหลทุติยภูมิในของไหลประเภทนิวโตเนียนและวิสโคอิลาติกผ่านท่อรูปทรงต่างๆ
นักศึกษา	นายทัพไทย สีเทา
รหัสประจำตัว	55612106
ปริญญา	วิศวกรรมศาสตรมหาบัณฑิต
สาขาวิชา	วิศวกรรมเคมี
พ.ศ.	2557
อาจารย์ที่ปรึกษาวิทยานิพนธ์	ดร.สันติ วัฒนานุสรณ์

บทคัดย่อ

การไหลทุติยภูมิเป็นลักษณะการไหลประเภทหนึ่งที่เกิดขึ้นในทางตัดขวางของท่อ การมีอยู่ของการไหลลักษณะนี้อาจส่งผลกระทบไปถึงตัวแปรต่างๆ อาทิ โปรไฟล์ความเร็ว ของการไหลหลักได้ ดังนั้นการศึกษา ทำความเข้าใจ ถึงการไหลทุติยภูมิจึงมีความสำคัญเป็นอย่างยิ่ง เพื่อที่จะนำองค์ความรู้ที่ได้รับไปใช้ออกแบบ พัฒนา เพิ่มประสิทธิภาพ ศักยภาพของเครื่องมือ กรรมวิธี กระบวนการผลิต รวมไปถึง คุณภาพของผลิตภัณฑ์ที่ได้รับจากกระบวนการผลิตนั้นๆอีกด้วย ในงานวิจัยนี้ได้ศึกษาถึงการไหลทุติยภูมิสำหรับของไหลสองประเภทประกอบด้วย ของไหลชนิดนิวโตเนียน และ ของไหลชนิดวิสโคอิลาสติก ผ่านท่อรูปทรงต่างๆด้วยการจำลอง ซึ่งผลการจำลองเบื้องต้นพบว่าการไหลทุติภูมิเกิดขึ้นเนื่องจากความไม่สมดุลของความเค้นในการไหลหลัก โดยเฉพาะความไม่สมดุลที่เกิดขึ้นจากเกรเดียนร์ของความดันที่ปรากฏขึ้นเมื่อท่อถูกทำให้โค้งงอ ระดับความแรงของการไหลทุติภูมิยังแปรผันตามความเร็วขาเข้าที่เพิ่มมากขึ้นในของไหลทั้งสองประเภท โดยในของไหลชนิดนิวโตเนียน การเพิ่มของระดับความแรงนี้จะส่งผลกระทบให้เกิดการดึงความเร็วในแนวตัดขวางเข้าสู่ศูนย์กลางของท่อ แต่สำหรับของไหลชนิดวิสโคอิลาสติก ปรากฏการณ์นี้จะเกิดขึ้นตรงข้ามกัน โดยจะเปลี่ยนจากศูนย์กลางเป็นมุมของท่อนั้นๆแทน

Thesis Title	Simulation of Secondary Flows in Newtonian and Viscoelastic Fluids through Various Shaped Conduits
Student	Mr. Tupthai Seethao
Student ID.	55612106
Degree	Master of Engineering
Program	Chemical Engineering
Year	2014
Thesis Advisor	Dr.Santi Wattananusorn

ABSTRACT

Secondary flows are the flow phenomena which occur in the transverse flow field of conduit. The occurrence of this phenomena may change many primary flow properties i.e., velocity profile. According to this chance, the understanding of secondary flows are required. In order to achieve the goal of many engineering applications which associate with the improvement of the efficiency and performance of the machines, equipment designs and product quality, the simulation of secondary flows for different fluid types through various shaped conduits were studied. The preliminary simulated results revealed that the secondary flow occurred by the unbalance of stresses in primary flow, especially, the unbalance from the presence of pressure gradient when conduits were bended. The secondary flow strength is proportional to an increase of inlet velocity of both fluid types. For Newtonian fluid, this increase also causes the induction of cross –stream velocity to the center of the conduit. In contrast with viscoelastic fluid which causes the induction to the corner of the conduit instead.

ACKNOWLEDGEMENTS

For my success, I wish to express my sincere thanks to the people who have contributed both directly and indirectly to this study. First of all, I would like to express my appreciation to my research advisor, Dr. Santi Wattananusorn, Department of Chemical Engineering, King Mongkut's Institute of Technology Ladkrabang, for deep discussion and encouraging guidance throughout the course of this work. Furthermore, all members of CFD's Group and my friends for their help, suggestion and warm collaborations. Last but not least, I would like to express my cordial and deep thanks to my family for their encouragement, understanding and huge support.

Tupthai Seethao

CONTENTS

Page

CONTENTS (Cont.)

CONTENTS (Cont.)

Page

CONTENTS (Cont.)

Page

LIST OF TABLES

Table Page

LIST OF FIGURES

Figure Page

LIST OF FIGURES (Cont.)

Figure Page

LIST OF FIGURES (Cont.)

Figure Page

NOMENCLATURE

Alphabetical Symbols

$D_{i,m}$	Mass diffusion coefficient for species i in the mixture (m^2 / s)
$\mathbf{D}$	Deformation rate tensor (s^{-1})
G	Rigidity modulus (Pa)
k	Thermal conductivity ($W / m \cdot K$)
l	Conduit length (m)
p	Pressure (Pa)
Δp	Pressure drop (Pa)
Q	Volumetric flow rate (m^3 / s)
R	Conduit radius (m)
S_M	Momentum source term
S_E	Total energy source term
S_{Mx}, S_{My}, S_{Mz}	Momentum source term in x, y, z directions
t	Time (s)
T	Temperature (K)
$\mathbf{T}$	Stress deviator tensor (Pa)
u, v, w	Velocity components in x, y, z directions (m / s)
$\mathbf{u}$	Velocity vector (m / s)
v_c	Maximum velocity (m / s)
x, y, z	Rectangular coordinates

Greek Symbols

α_K	Giesekus's non-linear parameter
λ_K	Relaxation time (s)
η_{P_K}	Polymeric viscosity ($Pa \cdot s$)
η_{S_s}	Solvent viscosity ($Pa \cdot s$)
ρ	Fluid density (kg/m^3)
σ , $\boldsymbol{\tau}$	Stress tensor (Pa)
δ_{ij}	3×3 Identical matrix
$\boldsymbol{\tau}_P$	Elastic polymeric contribution (Pa)
$\boldsymbol{\tau}_{P_K}$	Individual relaxation modes (Pa)
$\boldsymbol{\tau}_S$	Newtonian solvent contribution (Pa)
$\boldsymbol{\tau}_w$	Wall shear stress tensor (Pa)
$\tau_{xx}, \tau_{yy}, \tau_{zz}$	Normal stresses on x-x, y-y, z-z planes (Pa)
$\tau_{xy}, \tau_{xz}, \tau_{yz}$	Shear stresses on x-y, x-z, y-z planes (Pa)
γ	Strain
$\dot{\gamma}$	Strain-rate tensors (s^{-1})

CHAPTER I

INTRODUCTION

1.1 Background and Motivation

According to the advance of the current manufacturing and the capable technology, a vast range of fluid had been widely used in the productive activities to supply an increasing number of products in a wide range of industries such as food, pharmaceutical, polymer, chemical industries, in addition to applications in the oil, mining, construction, water treatment, power generation industries, etc. Examples of fluid used in industries include water, air, chemical substances, industrial oils, polymeric solutions, foams, organic and inorganic suspensions such as paints, and foodstuffs such as milk, yogurt, mayonnaise, juice and fruit and vegetable sauces.

Many enigmatic flow phenomena can be happened even though the flow is very simple because of the difference of fluid nature, chiefly, non-Newtonian fluids which are characterized by diverse and often significant deviations from simple Newtonian behavior. To achieve the goal of every engineer, understanding of fluid flow phenomena is very important to improve the efficiency and performance of the machines, equipment designs and product quality, especially, the flow regions where the speed and direction of flow are significantly different. This flow phenomena is also known as "The Secondary Flow".

In cases where there is a three-dimensional flow field, the flow is often regarded as comprising two components, a primary flow and a secondary flow. The primary flow is parallel to the main direction of fluid motion and the secondary flow is perpendicular to this. Such flows are commonly produced by the effect of drag in the boundary layers, and some of the more important situations. Many researchers had been discussed in the presence of secondary flow to gain insight into this phenomena for example, Xue et al. [1] investigated numerically the pattern and strength of the secondary flows in rectangular pipes as well as the influence of material parameters on them, Letelier and Siginer [2] studied about the unsteady flow of the Green–Rivlin fluids in straight tubes of arbitrary cross-section driven by a pulsating pressure gradient in 2003 and so on. For bring the advantage of secondary flow into many applications,

the understanding of its mechanism and occurrence is required. Nonetheless, this study refers to the conditions of the flow domain which can build-up the secondary flow along with their flow pattern and strength.

Computational Fluid Dynamics (CFD) is a branch of fluid mechanics that uses numerical method and algorithm to solve and analyze momentum, heat, and mass transfer in various systems. Phenomena of fluid flow are usually explained by three fundamental physical laws, including the conservation of mass, the Newton's second law of motion, and the first law of thermodynamics. This techniques is a useful tool for studying fluid flow motion. CFD have been applied on a broad scale in the process industry to gain insight into various flow phenomena, examine different equipment designs or compare performance under different operating conditions.

Regarding to the benefits of CFD and requirement of the understanding of secondary flow appearance, the flows with two type of fluid including Newtonian fluid and Viscoelastic fluid through various shapes of conduit has been studied. The flow is assumed to be laminar and incompressible. The effect of different conduit geometries has been investigated by the CFD modeling and predicted hydrodynamics parameters have been used to explain the observed results.

1.2 Objectives of the Research

The research reported in this thesis aims to investigate the secondary flow behavior in Newtonian and viscoelastic Fluids through various shaped conduits and inlet velocity by using simulation through OpenFOAM®.

1.3 Scope of the Research

1.3.1 *Validation of simulation setting* by compare between calculated flow rate and velocity profile from theoretical for Newtonian fluid and previous simulated result for viscoelastic fluid.

1.3.2 *Employ CFD technique to investigate the occurrence of secondary flows including their pattern, velocity magnitude, and their strength that were occurred in different conditions of flow domain and fluid properties* including:

a) Cross-sectional shapes of conduit including circular, elliptical, triangular, square, hexagonal, and octagonal.
b) The difference between straight conduit and curved conduit. In addition, their orientations when conduits were bended.
c) The initial velocities which in the range of laminar flow.
d) Fluid type; Newtonian fluid and viscoelastic fluid.

1.4 Process of the research

1) Conduct literature survey and review.
2) Define the simulation and collect all necessary data required.
3) Model setup (e.g. Solid modeling, grid generation, etc.).
4) Investigate grid independent solutions.
5) Validate the simulation results with literature data and previous CFD simulation for confirm the correcting of simulation setup and the numerical solution process.
6) Simulation of parameters which effect on the occurrence of secondary flow along with collect desired information for the analysis.
7) Making discussion and conclusion of simulation results.
8) Writing thesis and preparation of draft manuscript for journal publication.

1.5 Expected Benefit

Obtain knowledge of secondary flow and its appearance in different flow domain conditions by using OpenFOAM®.

CHAPTER II

THEORY AND LITERATURE REVIEW

2.1 Computational Fluid Dynamics (CFD)

Computational Fluid Dynamics (CFD) is the analysis tool that use computer aided simulation to solve and analyze systems involving the fluid flow, heat transfer and associated phenomena such as chemical reaction [3]. Fluid flow motion which describe by a set of mathematical equations are solved by numerical methods and algorithms in order to obtain the flow variables throughout the flow domain.

CFD can be applied in a wide range of processes and applications in academic researches or in industries such as mechanical, petroleum, metallurgical, biomedical, pharmaceutical, and food industries. CFD becomes an important and useful engineering tool because this techniques have been applied on a broad scale in the process industry to gain insight into various flow phenomena, examine different equipment designs or compare performance under different operating conditions. Examples of CFD applications in the chemical process industry include drying, combustion, separation, heat exchange, mass transfer, pipeline flow, reaction, mixing, multiphase systems and material processing.

CFD has also been successfully used in modelling various type of fluid including Newtonian fluid and non-Newtonian fluid. CFD models can help understand their flow phenomenon, especially invisible behavior, and provide detailed 3-D transient data that experimental approaches may not be able to provide.

2.1.1 Advantages of CFD

Since 1960s, the aerospace industry has integrated CFD techniques into design and manufacturing of aircraft and jet engines. The further growth and development in CFD together with the rapid increasing in computer capability have constantly expanded the range of CFD applications. Nowadays, CFD has been interested and has been widely used to study various aspects of fluid dynamics. The development and application of CFD technique have undergone considerable growth, and as a result,

it has become a powerful tool in the design and analysis of engineering and other processes.

Although the use of CFD and their results may have the degree of uncertainty and the cumulative effect of various errors such as the lack of knowledge or Computer programming error. However, these errors are far overweighed by benefits of CFD [4] and can be reduced by the awareness of the error sources. Nonetheless, a number of CFD advantages include the following:

i. CFD simulation is less expensive and time consuming compare with doing experiment along with its ability to study systems where controlled experiments are not feasible.
ii. CFD can provide a wide range of comprehensive data as no such limitations such as equipment or technique limitations are usually present.
iii. The complex physical interactions which occur in a flow situation can be modelled simultaneously since no limiting assumptions are usually needed.
iv. CFD can provide comprehensive flow visualization for many industrial applications and academic research to improve the design and optimize different processes and devices working with fluid flows.

2.1.2 CFD Analysis Procedure

The CFD analysis procedure can be described as the following stages;

i. Problem statement

The understanding of the problem is needed in order to define the simulation and collect all necessary data required including geometry details, fluid properties and flow specifications.

ii. Geometry creation and mesh generation

a) The geometry of fluid flow domain is created into 2-D or 3-D sketches.
b) The computational domain is divided into sufficiently small discrete cells which determines the positions where the flow variables are to be calculated and stored.

iii. Mathematical model

a) Identify the force which cause and influence the fluid motion.

b) Formulate conservation laws for the mass, momentum, and energy.

c) Simplify the governing equations to reduce the computational effort such as neglect the terms which have little or no influence on the results.

d) Add constitutive relations and specify initial/boundary conditions.

iv. Discretization process

The Partial Difference Equations (PDEs) system is transformed into a set of algebraic equations with appropriate methods.

v. Calculation of the numerical solution

a) The CFD software performs iterative calculations to arrive at a solution to the numerical equations representing the flow.

b) The quality of simulation results depends on the information that control the numerical solution process such as the mathematical model, underlying assumptions, approximation type, or convergence criteria.

vi. Result analysis

Analyzing of simulation results is performed in order to extract the desired information from the computed flow field. If the results obtained are unsatisfactory, the possible source of error needs to be identified, which can be an incorrect flow specification, a poor mesh quality, or a conceptual mistake in the formulation of the problem [5].

Typically, CFD procedure can be distinguished by the type of CFD software package which consists of three main groups of software including a pre-processer, a solver, and a post-processer.

Pre-processing

Pre-processing consist of the input of flow problem including geometry and mesh generation, flow specification, selection of the physical and chemical phenomena, definition of material properties, and setting solver control parameters.

Solving the equations

In this step, all the data defined in the pre-processing step are fed into the solver program in the form of a data file. Then, the solver solves the numerical equations which transform into algebraic equations form. There are three distinct streams of numerical solution technique, including finite difference method, finite element method, and finite volume methods for chosen to use in this step

Post-Processing

In post processing, the data obtained by the solver can be visualized and displayed using a variety of data visualization tools such as contour, plane, vector and line plots. Calculations can also be made to obtain the values of scalar and vector variables, such as pressure and velocity, at different locations.

CFD procedure can be summarized by the type of software package as a diagram, which shown in Figure 2.1.

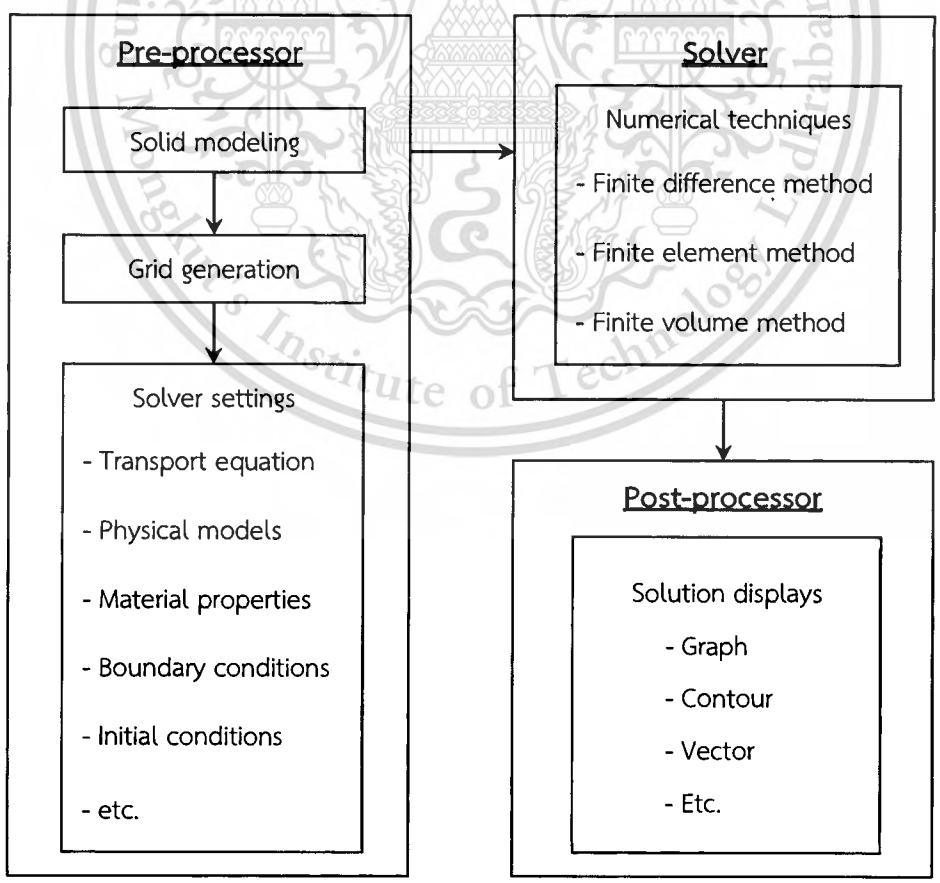

Figure 2.1 CFD processing diagram.

2.1.3 Finite Volume Method (FVMs)

The finite volume method is probably the most popular method used for numerical discretization in CFD because this method was originally developed as a special finite difference formulation but some of its implementations draw on features taken from the finite element method.

This method involves the discretization of the flow domain into finite control volumes. A control volume overlaps with many mesh elements and can be divided into sectors each of which belongs to a different mesh element.

The governing equations in their differential form are integrated over each control volume. The resulting integral conservation laws are exactly satisfied for each control volume and for the entire domain which is a distinct advantage of this method. Then, each integral term is converted into a discrete form (a set of algebraic equations), thus providing discretized equations at the centroids, or nodal points, of the control volumes as shown in Figure 2.2

Figure 2.2 Mesh and dual mesh of two FVMs: (a) centroids FVM and (b) nodal points FVM [6].

2.2 Governing Equations

The governing equations are a set of mathematical equations which explain the physical phenomena by the conservation laws of physics [3] involving:

1) Mass of fluid is conserved.
2) According to Newton's second law on a fluid particle or control volume summation of the forces are equal to the rate of the momentum change.
3) According to the first law of thermodynamics the rate of energy change equals to the heat rate added to the control volume or the fluid particle and the rate of the work done on the fluid particle.

2.2.1 Mass Conservation Equation

According to the mass conservation which is based on the statement "mass may be neither created nor destroyed", the rate of the mass increase in fluid element is equal to the net rate of the flow into the fluid element. For the compressible flow this can be formulated as follows and is called the continuity equation for an unsteady compressible fluid at a point;

$$\frac{\partial \rho}{\partial t}+\frac{\partial}{\partial x}(\rho u)+\frac{\partial}{\partial y}(\rho v)+\frac{\partial}{\partial z}(\rho w)=0 \tag{2.1}$$

or

$$\frac{\partial \rho}{\partial t}+\nabla\cdot(\rho \mathbf{U})=0 \tag{2.2}$$

where $\mathbf{U}$ is the velocity vector in Cartesian coordinate and given by

$$\mathbf{U}=u\mathbf{i}+v\mathbf{j}+w\mathbf{k}$$

where $\mathbf{i}$, $\mathbf{j}$, and $\mathbf{k}$ are the unit vectors along x, y, and z axes, respectively.

2.2.2 Momentum Conservation Equations

According to the second law of Newton, the time rate of change of momentum of a system is equal to the net force acting on the system and takes place in the direction of the net force. Actually there are two different types of forces that act in any fluid:

1) Long ranged external body forces that penetrate matter and act equally on all the material in any element.
2) Short ranged molecular forces, internal to the fluid. For any element, the net effect of these due to interactions with other elements acts in a thin surface layer. In 3D, each of the 3 sets of surface planes bounding an element experiences a 3-component force, giving 9 components in all. These form the stress tensor (τ_{ij}), defined so the force exerted per unit area across a surface element.

Thus, the three momentum conservation equations are given by;

The momentum equation in the x direction:

$$\rho\frac{Du}{Dt}=\frac{\partial(\rho u)}{\partial t}+\nabla\cdot(\rho u\mathrm{U})=-\frac{\partial p}{\partial x}+\frac{\partial\tau_{xx}}{\partial x}+\frac{\partial\tau_{yx}}{\partial y}+\frac{\partial\tau_{zx}}{\partial z}+S_{Mx} \qquad (2.3)$$

The momentum equation in the y direction:

$$\rho\frac{Dv}{Dt}=\frac{\partial(\rho v)}{\partial t}+\nabla\cdot(\rho v\mathrm{U})=-\frac{\partial p}{\partial y}+\frac{\partial\tau_{xy}}{\partial x}+\frac{\partial\tau_{yy}}{\partial y}+\frac{\partial\tau_{zy}}{\partial z}+S_{My} \qquad (2.4)$$

The momentum equation in the z direction:

$$\rho\frac{Dw}{Dt}=\frac{\partial(\rho w)}{\partial t}+\nabla\cdot(\rho w\mathrm{U})=-\frac{\partial p}{\partial z}+\frac{\partial\tau_{xz}}{\partial x}+\frac{\partial\tau_{yz}}{\partial y}+\frac{\partial\tau_{zz}}{\partial z}+S_{Mz} \qquad (2.5)$$

2.2.3 Energy Conservation Equations

According to the law of thermodynamics state that if a system is carried through a cycle, the total heat added to the system from its surroundings is proportional to the work done by the system on its surroundings and that lead to the corresponding relation which the energy change rate for a fluid particle is the rate of work done on the fluid particle in addition to the heat added. The energy equation in term of total energy (E) is given by;

$$\rho\frac{DE}{Dt}=-\frac{\partial(up)}{\partial x}-\frac{\partial(vp)}{\partial y}-\frac{\partial(wp)}{\partial z}+\frac{\partial}{\partial x}\left(k\frac{\partial T}{\partial x}\right)+\frac{\partial}{\partial y}\left(k\frac{\partial T}{\partial y}\right)+\frac{\partial}{\partial z}\left(k\frac{\partial T}{\partial z}\right)$$

$$+\frac{\partial(u\tau_{xx})}{\partial x}+\frac{\partial(u\tau_{yx})}{\partial y}+\frac{\partial(u\tau_{zx})}{\partial z}+\frac{\partial(v\tau_{xy})}{\partial x}+\frac{\partial(v\tau_{yy})}{\partial y}+\frac{\partial(v\tau_{zy})}{\partial z}$$

$$+\frac{\partial(w\tau_{xz})}{\partial x}+\frac{\partial(w\tau_{yz})}{\partial y}+\frac{\partial(w\tau_{zz})}{\partial z}+S_E \qquad (2.6)$$

The term E consists of internal energy i and the kinetic energy. The S_E term is the energy term related to a source. The term including the temperature gradient is the heat transfer to the fluid and the rest terms of the right side are the work done on the fluid particle.

2.2.4 Navier-Stokes equations

The Navier-Stokes equations, developed by Claude-Louis Navier and George Gabriel Stokes in 1822, are equations which can be used to determine the velocity vector field that applies to a fluid, given some initial conditions. They arise from the application of Newton's second law in combination with a fluid stress (due to viscosity) and a pressure term to fluid motion, which the general form of the Navier-Stokes equation is;

$$\rho\frac{DU}{Dt}=\nabla\cdot\sigma+\mathrm{f} \tag{2.7}$$

where σ is stress tensor and f accounts for other body forces present.

The stress tensor is often divided into two terms of interest in the general form of the Navier-Stokes equation. The two terms are the volumetric stress tensor, which tends to change the volume of the body, and the stress deviator tensor, which tends to deform the body. The volumetric stress tensor represents the force which sets the volume of the body (namely, the pressure forces). The stress deviator tensor represents the forces which determine body deformation and movement, and is composed of the shear stresses on the fluid. Thus, the stress tensor is broken down into;

$$\sigma=\begin{pmatrix}\sigma_{xx} & \tau_{xy} & \tau_{xz}\\ \tau_{yx} & \sigma_{yy} & \tau_{yz}\\ \tau_{zx} & \tau_{zy} & \sigma_{zz}\end{pmatrix}=-\begin{pmatrix}p & 0 & 0\\ 0 & p & 0\\ 0 & 0 & p\end{pmatrix}+\begin{pmatrix}\sigma_{xx}+p & \tau_{xy} & \tau_{xz}\\ \tau_{yx} & \sigma_{yy}+p & \tau_{yz}\\ \tau_{zx} & \tau_{zy} & \sigma_{zz}+p\end{pmatrix}$$

$$=-p\delta_{ij}+T \tag{2.8}$$

where δ_{ij} is the 3×3 identical matrix and T is the stress deviator tensor

Although this is the general form of the Navier-Stokes equation, it cannot be applied until it has been more specified. First off, depending on the type of fluid, an expression must be determined for the stress tensor T; secondly, if the fluid is not assumed to be incompressible, an equation of state and an equation dictating conservation of energy are necessary.

By the expression which assume the relationship between stress and velocity gradients is

a) Linear relation of the rate of the deformation to the viscous stresses (which is valid for Newtonian fluids) and
b) Isotropic (i.e., the intrinsic properties of the fluid have no preferred direction)

In result the three dimensional tensor of stress can be gained:

$$\tau_{xx} = -p + \lambda \nabla \cdot \mathrm{U} + 2\mu \frac{\partial u}{\partial x} \qquad \tau_{xy} = \tau_{yx} = \mu \left(\frac{\partial u}{\partial y} + \frac{\partial v}{\partial x} \right) \tag{2.9}$$

$$\tau_{yy} = -p + \lambda \nabla \cdot \mathrm{U} + 2\mu \frac{\partial v}{\partial y} \qquad \tau_{yz} = \tau_{zy} = \mu \left(\frac{\partial v}{\partial z} + \frac{\partial w}{\partial y} \right) \tag{2.10}$$

$$\tau_{zz} = -p + \lambda \nabla \cdot \mathrm{U} + 2\mu \frac{\partial w}{\partial z} \qquad \tau_{xz} = \tau_{zx} = \mu \left(\frac{\partial u}{\partial z} + \frac{\partial w}{\partial x} \right) \tag{2.11}$$

where μ and λ are the coefficients of dynamic and bulk viscosity respectively.

Then by substituting these stress tensor to the momentum equations, the Navier-Stokes equations can be gained;

x -momentum:

$$\frac{\partial (\rho u)}{\partial t} + \nabla \cdot (\rho u \mathrm{U}) = -\frac{\partial p}{\partial x} + \mu \left(\frac{\partial^2 u}{\partial x^2} + \frac{\partial^2 u}{\partial y^2} + \frac{\partial^2 u}{\partial z^2} \right) + S_{Mx} \tag{2.12}$$

y -momentum:

$$\frac{\partial (\rho v)}{\partial t} + \nabla \cdot (\rho v \mathrm{U}) = -\frac{\partial p}{\partial x} + \mu \left(\frac{\partial^2 v}{\partial x^2} + \frac{\partial^2 v}{\partial y^2} + \frac{\partial^2 v}{\partial z^2} \right) + S_{My} \tag{2.13}$$

x -momentum:

$$\frac{\partial (\rho w)}{\partial t} + \nabla \cdot (\rho w \mathrm{U}) = -\frac{\partial p}{\partial x} + \mu \left(\frac{\partial^2 w}{\partial x^2} + \frac{\partial^2 w}{\partial y^2} + \frac{\partial^2 w}{\partial z^2} \right) + S_{Mz} \tag{2.14}$$

2.2.5 Constitutive equations

Constitutive equation or constitutive relation is a relation between two physical quantities, mostly kinetic quantities as related to kinematic quantities, which is specific to a material or substance, and approximates the response of that material to external forces. Constitutive equations are combined with other equations governing physical laws to solve physical problems; for example in fluid mechanics the flow of a fluid in a pipe, in solid state physics the response of a crystal to an electric field, or in structural analysis, the connection between applied stresses or forces to strains or deformations.

2.2.5.1 Viscoelasticity

Viscoelasticity is a rheological parameter that describes the flow properties of complicated structure or complex fluid. There are two components to the viscoelasticity, the viscosity and the elasticity. This parameter was further examined in the late twentieth century when synthetic polymers were engineered and used in a variety of applications. Many viscoelastic materials exhibit rubber like behavior explained by the thermodynamic theory of polymer elasticity. In reality all materials deviate from Hooke's law in various ways, for example by exhibiting viscous-like as well as elastic characteristics.

Viscoelasticity is a time-dependent mechanical response to loading exhibited by most often by amorphous materials. In its simplest conception, viscoelasticity consists of a combination of time independent elastic behavior and time dependent viscous behavior.

All materials exhibit some viscoelastic response. In common metals such as steel or aluminum, as well as in quartz, at room temperature and at small strain, the behavior does not deviate much from linear elasticity. Synthetic polymers, wood, and human tissue as well as metals at high temperature display significant viscoelastic effects. In some applications, even a small viscoelastic response can be significant. To be complete, an analysis or design involving such materials must incorporate their viscoelastic behavior. Knowledge of the viscoelastic response of a material is based on measurement.

Some examples of viscoelastic materials include amorphous polymers, semi-crystalline polymers, biopolymers, metals at very high temperatures, and bitumen materials.

2.2.5.2 Constitutive equations for viscoelastic fluids

General linear viscoelastic model

Viscoelastic fluids are often described by equations based on the following or similar forms [7]:

$$\tau = f\left(\gamma, \dot{\gamma}, t\right) \tag{2.15}$$

where τ , γ , and $\dot{\gamma}$ are the stress, strain, and strain-rate tensors, respectively. According to this relation, the shear stress in a viscoelastic fluid may be a function of the strain (characteristic of solids), the rate of strain (characteristic of liquids), and time. General linear viscoelastic model is simple model to describe viscoelastic behavior and it is restricted to materials that are subject to small deformations and small deformation rates (linear viscoelastic regime).

The Maxwell model

The Maxwell model, which serves mainly as an introduction to viscoelasticity, incorporates both of viscous liquids and elastic solids, and is best introduced by considering again the case of simple shear, shown in Figure 2.3, but this time for either a fluid *or* a solid. For simplicity, assume that $\tau = \tau_{yx}$ is constant.

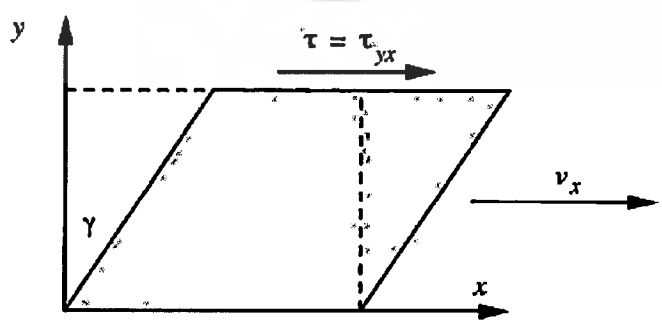

Figure 2.3 Simple shear of a fluid or solid (γ exaggerated) [7].

Assuming that the deformation γ is small, the two extremes of behavior are represented by a Newtonian fluid, of viscosity η (= μ), and a Hookean elastic solid, whose rigidity modulus (G):

Newtonian fluid

$$\tau = \eta \frac{dv_x}{dy} = \eta \frac{d\gamma}{dt} = \eta\dot{\gamma} \tag{2.16}$$

Hookean elastic solid

$$\tau = \gamma G \quad or \quad \dot{\gamma} = \frac{d\gamma}{dt} = \frac{1}{G}\frac{d\tau}{dt} \tag{2.17}$$

The Maxwell model then views the total strain rate as the sum of the strain rates for the Newtonian fluid and Hookean solid, resulting in the following constitutive equation:

$$\frac{\tau}{\eta} + \frac{1}{G}\frac{d\tau}{dt} = \dot{\gamma} \tag{2.18}$$

Although η and G both increase in progressing from liquids to solids, η increases faster than G, so the overall effect is an increase in the ratio $\lambda = \eta/G$, which is known as the relaxation time, and is low for fluids and high for solids. The basic reason is stresses in liquids can relax more quickly than those in solids because of the higher mobility of the liquid molecules. In terms of λ, the Maxwell model becomes:

$$\tau + \lambda\frac{d\tau}{dt} = \eta\frac{d\gamma}{dt} = \dot{\gamma} \tag{2.19}$$

The principle of the Maxwell model is shown schematically in Figure 2.4. The Newtonian behavior of the fluid is represented by a "dashpot," which the force is proportional to the rate of extension. The dashpot is in series with an elastic spring that represents the Hookean behavior of the fluid which the force is proportional to the extension. Note that the Maxwell model is restricted to deformations that are small, so that the response of the fluid is linear—a phenomenon known as linear viscoelasticity.

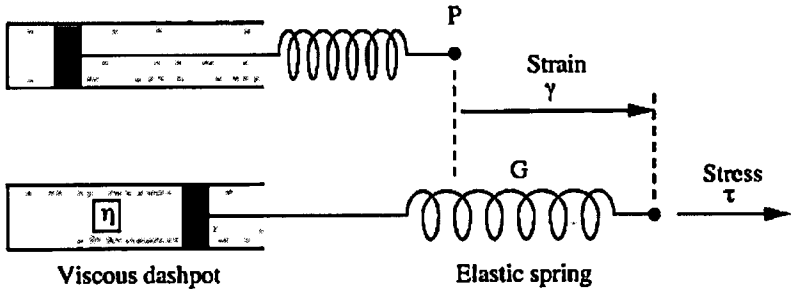

Figure 2.4 The Maxwell model of linear viscoelasticity [7].

The Maxwell model makes the following realistic predictions:

I. Steady shear causes flow.

II. If the strain no longer changes, $\frac{d\gamma}{dt}=0$, then the stress relaxes from its maximum value τ_0 according to:

$$\tau=\tau_0 e^{-Gt/\eta}=\tau_0 e^{-t/\lambda} \tag{2.20}$$

from which the relaxation time λ is clearly the time taken for the stress to fall to 1/e = 36.8% of its initial value.

III. If the stress is removed, so that τ = 0, there will be some recoil or elasticity.

Equation (2.19) is a first-order linear differential equation that can be solved to yield an expression for the shear-stress τ :

$$\tau(t)=\int_{-\infty}^{t}\left[\frac{\eta}{\lambda}e^{-(t-t')/\lambda}\right]\dot{\gamma}(t')dt' \tag{2.21}$$

The stress in the fluid is a function not only of the strain rate at the current time t but also of the strain rate at previous times, designated by t'. The term in brackets is *the relaxation modulus* G, which weights the effect of the strain rate at previous times less than t. Note that the relaxation modulus equals unity when $t=t$ and is equal to zero when $t=\infty$. Consequently, the fluid has a "memory" of past deformations, which decays exponentially with time.

The shear-stress can also be written in terms of the difference $\left[\gamma(t)-\gamma(t')\right]$ between the strains at times t and t':

$$\tau(t)=\int_{-\infty}^{t}\left[\frac{\eta}{\lambda^2}e^{-(t-t')/\lambda}\right]\left[\gamma(t)-\gamma(t')\right]dt' \tag{2.22}$$

The quantity in brackets is *the memory function*, which describes the effect of strain prehistory on the stress.

Other Constitutive Equation for viscoelastic fluid

From the principle of the Maxwell model, many constitutive equations have been proposed for polymeric fluids, and many have been discarded. A few of them survived and are currently receiving attention. Some of more accurate constitutive equations are shown as the following;

The Oldroyd 8-Constant Model or The upper-convected Maxwell (UCM) model

This model proposed by James G. Oldroyd (1958). It is an empirical expression that is linear in the stress tensor, but contains all allowable terms quadratic in velocity gradients and all allowable products of stresses and velocity gradients. Since it can give qualitatively correct results in a wide variety of flow situations, it has been popular for developing the numerical techniques for non-Newtonian fluid dynamics.

The Giesekus Model

Giesekus (1982), using molecular ideas, developed a three-constant ($\eta_0, \lambda_1, \alpha$) model that is nonlinear in the stresses. This model has gained prominence because it describes the power-law regions for viscosity and normal-stress coefficients; it also gives a reasonable description of the elongational viscosity and the complex viscosity.

The Phan-Thien-Tanner Model

The four-constant model of Phan-Thien & Tanner (1977) and Phan-Thien (1978) was derived from a network theory for polymer melts and is also nonlinear in the stresses.

The FENE (Finitely-Extensible-Nonlinear-Elastic) Dumbbell Model

2.3 Newtonian Fluid and non – Newtonian Fluid

Nowadays, many types of fluid were used in the manufacturing of many industries. The rheology of them are characterized by theirs flow curve, which represents the relationship between shear stress and shear rate. The ratio of shear stress to shear rate is the fluid apparent viscosity, as shown in Figure 2.5.

A Newtonian fluid is characterized by a linear flow curve which passes through the origin. The viscosity of such a fluid is constant and independent of shear rate. Examples of Newtonian behavior include water, air, and most aqueous solution etc.

A non- Newtonian fluid is a fluid whose flow curve is non-linear or/and does not pass through the origin. The apparent viscosity of such a fluid depends on the shear rate, which is variable in shear flow. More complex non-Newtonian fluids have an apparent viscosity which depends on the duration of shearing and the kinematic history of the fluid, and are described as time dependent. The behavior of a non-Newtonian fluid can be related to the behavior of a hypothetical Newtonian fluid using the concept of effective viscosity, Examples of non-Newtonian behavior include paint, many polymer solution, molten polymer, many solid suspensions, blood, and most highly viscous fluids etc.

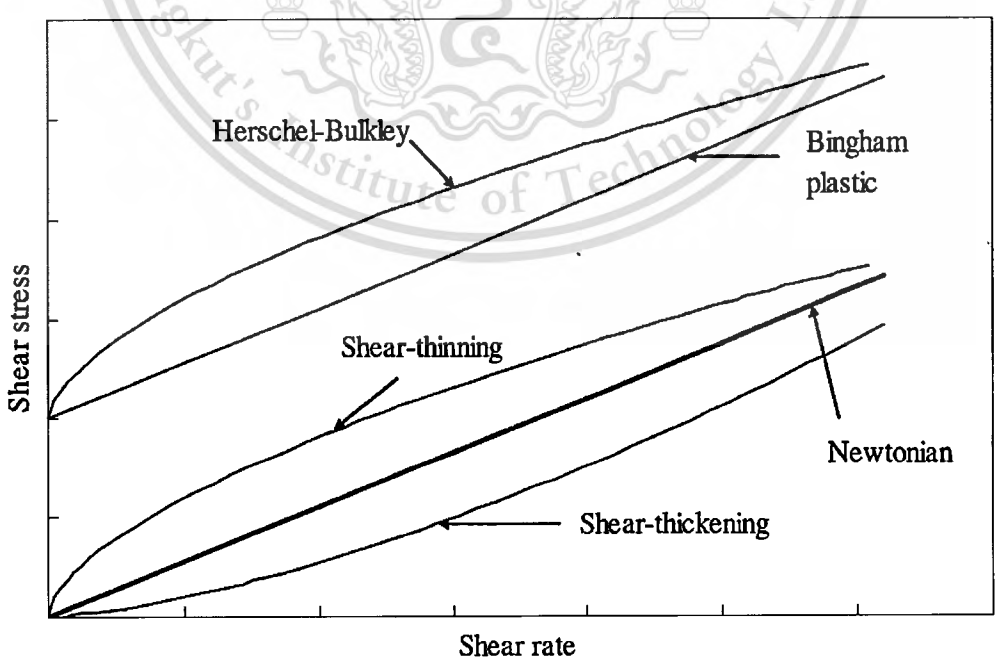

Figure 2.5 Flow curves for Newtonian and non-Newtonian fluids [6].

2.3.1 Newtonian Fluid

Newtonian fluid is any fluid which their viscosity remains constant regardless of velocity of the flow or any external stress that is placed upon it, such as mixing or a sudden application of force. Another way to describe these fluids is that they have a linear relationship between viscosity and shear stress. Regardless of the shear stress applied to these fluids, the coefficient of viscosity will not change.

Newtonian fluids are named after Isaac Newton, who first derived the relation between the rate of shear strain rate and shear stress for such fluids in differential form. They are the simplest mathematical models of fluids that account for viscosity. While no real fluid fits the definition perfectly, many common liquids and gases, such as water, vegetable oils, milk, and air, can be assumed to be Newtonian for practical calculations under ordinary conditions.

It is possible to change the viscosity of a Newtonian fluid, if it is exposed to different temperatures or pressures instead of external applications of force. Many fluids become thicker as they are cooled, for example, Compressible liquids will tend to become thicker under pressure, while incompressible liquids exhibit a negligible change under the same circumstances. These fluids can also change in density when exposed to extreme temperatures, which can lead to an increase or decrease in viscosity. A fluid that has changed viscosity through one of these methods will still show a linear relationship between viscosity and shear stress.

2.3.2 Non-Newtonian Fluid

A non-Newtonian fluid is a fluid whose flow properties differ in any way from those of Newtonian fluids. Most commonly the viscosity of non-Newtonian fluid is variable based on applied stress. In a non-Newtonian fluid, the relation between the shear stress and the shear rate is different and can even be time-dependent. The flow curve of non – Newtonian fluid is either non-linear, or does pass through the origin, or both.

Non-Newtonian fluids can be classified into 3 classes by their behavior;

1) *Time – independent viscosity*

Fluids which the rate of shear at any point is determined only by the value of the shear stress at that point; these fluids are variously known as "time independent", "purely viscous", "inelastic", or "Generalized Newtonian Fluids" (GNF).

2) Time – dependent viscosity

More complex fluids for which the relation between shear stress and shear rate depends, in addition, on the duration of shearing and their kinematic history; they are called "time-dependent fluids".

3) Viscoelastic

Substances exhibiting characteristics of both ideal fluids and elastic solids and showing partial elastic recovery, after deformation; these are characterized as "viscoelastic" fluids.

Types of non-Newtonian behavior are depicted in Figure 2.6 and the summary are show in table 2.1

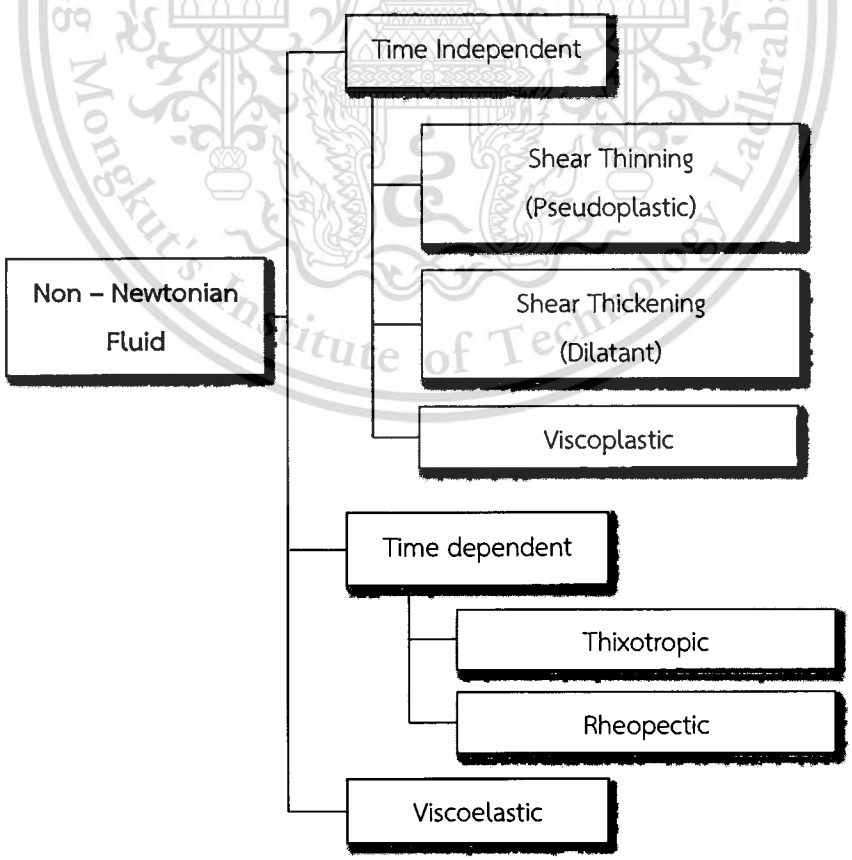

Figure 2.6 Types of non-Newtonian behavior.

Table 2.1 Type of non-Newtonian fluid behavior.

Type		Property	Example
Time Independent	Shear thinning (Pseudoplastic)	Apparent viscosity *decreases* with increased stress (Over a limited range of shear or stress rate)	polymer melts and solutions, protein concentrates, cream
	Shear Thickening (Dilatant)	Apparent viscosity *increases* with increased stress (observed in concentrated solid-liquid suspensions)	corn starch in water, sand in water
	Viscoplastic (Bingham, Herschel-Bulkley)	Fluid do not appear to flow until the shear stress exceeds (the yield stress)	tooth paste, tomato paste
Time dependent	Thixotropic	Apparent viscosity *decreases* with duration of stress	yogurt, paints, colloidal suspensions
	Rheopectic	Apparent viscosity *increases* with duration of stress	printer ink, gypsum paste
Viscoelastic		Combination of elastic and viscous effects (viscoelasticity)	lubricants, many of polymer, blood [8]

2.3.3 Viscoelastic Fluid

The phenomena of viscoelastic fluid, which occurred from the additional of elastic behavior, can be described by the constitutive equation as reported in section 2.2.5.2 constitutive equations for viscoelastic fluid. For several additional phenomena of viscoelastic fluids [7] are illustrated in Figure 2.7.

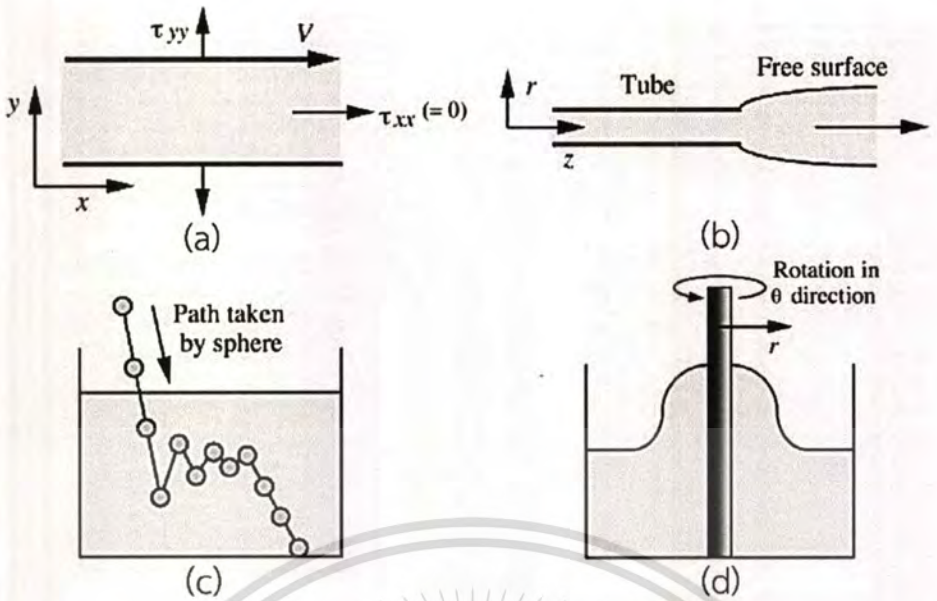

Figure 2.7 Characteristics of viscoelastic fluid; (a) Normal – stress effect, (b) Die swell, (c) Elastic recoil, and (d) Rod climbing [7].

(a) Normal –stress effect ($N_1 = \tau_{xx} - \tau_{yy}$): When apply simple shear between two plates which τ_{xx} is zero. Form the relationship of normal – stress, τ_{yy} must be negative which indicate a compressive stress, similar to pressure, that to push the two plates apart.

(b) Die swell: When polymer flow in tube, the polymer molecules in the direction of flow were straighten by flow motion. However, after these molecules are released from the confines of the tube, they attempt to return to their original, therefore "expanding" (the fluid is incompressible and its total volume is unchanged) in the radial direction with a consequent reduction in the axial velocity.

(c) Elastic recoil: When the sphere was dropped into the fluid, it has been given some artificial horizontal motion so that its up-and-down movement can readily be visualized before settling slowly and steadily to the bottom [9].

(d) Rod climbing: If a viscoelastic fluid is stirred by a rotating rod, it shows the rod-climbing or Weissenberg effect [10]. The stirring tends to straighten out the polymer molecules in the direction of rotation; however, these molecules attempt to return to their original configuration, thereby creating a tensile hoop stress.

2.4 Laminar Flow

Laminar or Streamline Flow, is a well-ordered flow and is characterized by the smooth sliding of thin fluid layers (*or lamina*), which these layer can be curved or straight depending on the flow of the fluid, over one another. There are no cross currents perpendicular to the direction of flow, nor eddies or swirls of fluids.

When a fluid is flowing through a closed channel such as a pipe or between two flat plates, either of two types of flow may occur depending on the velocity of the fluid: *laminar flow or turbulent flow*. Laminar flow tends to occur at lower velocities, in contract to turbulent flow, in which the fluid is a less orderly flow regime that is characterized by eddies or small vortices which induce to the lateral mixing [11]. In nonscientific terms laminar flow is "smooth", while turbulent flow is "rough" as show in Figure 2.8.

Figure 2.8 The type of fluid flow; (a) Laminar flow and (b) turbulent flow [12].

The type of fluid flow is very important in fluid dynamics problems and it can be characterized by the dimensionless Reynolds number. The Reynolds number ($\mathbf{Re}$) is an important parameter to describe the flow conditions lead to laminar or turbulent flow. The Reynolds number delimiting laminar and turbulent flow depends on the particular flow geometry, and moreover, the transition from laminar flow to turbulence can be sensitive to disturbance levels and imperfections present in a given configuration.

When the Reynolds number is much less than 1, creeping motion or Stokes flow occurs. This is an extreme case of laminar flow where viscous (friction) effects are much

greater than inertial forces. In creeping flow the nonlinear momentum terms are unimportant, and the Navier-Stokes equation can be linearized.

Laminar flow is common only in cases in which the flow channel is relatively small, the fluid is moving slowly, and its viscosity is relatively high such as oil flow through a thin tube or blood flow through capillaries is laminar. Most other kinds of fluid flow are turbulent except near solid boundaries, where the flow is often laminar, especially in a thin layer just adjacent to the surface. For example, the flow of air over an aircraft wing. The boundary layer is a very thin sheet of air lying over the surface of the wing (and all other surfaces of the aircraft). Because of air's viscosity, the layer of air tends to attach to the wing. As the wing moves forward through the air, the boundary layer at first flows smoothly over the streamlined shape of the airfoil. At this region, the flow is called laminar and their boundary layer is also called laminar boundary layer.

2.5 Secondary Flow

2.5.1 Definition of Secondary Flow

For three – dimensional flow flied, the flow is often regarded as comprising two components, a primary flow and a secondary flow. Secondary flow is a name for time – mean flow motion which embedded in a primary flow. There are many variants of this phenomena. Some judgment is needed in distinguishing two elements. Firstly, the secondary flow velocities are considerably smaller than those of the basic motion. Secondly, when the primary motion is parallel to a wall or to a uniform free stream, secondary element is taken to be the cross-channel or cross-stream component of the mean flow [13].

2.5.2 Types of Secondary Flows [13]

Type 1 – the cross-channel component of a fully developed flow in a channel with parallel walls: This type of secondary flow develops when the direct mixing stresses in the cross-section are not self – equilibrating, and is of special interest because it derives directly from turbulent activity. Form cross-sectional velocity contour, the variation of velocities over the core of a turbulent flow is proportionally smaller than that for laminar flow in the same channel. This effect is accentuated

by *secondary flows*, which act to extend the core into the angles of the section. Consequently, for a channel section whose corners are not too shape, the wall layer and shear stress are fairly uniform around much of the perimeter.

Other kinds of secondary flow, which can occur in the absence of turbulence or interact with turbulence when it is present, are distinguished as the following;

Type 2 – the flow in the cross – section of a curved channel inwards near the wall, and outwards in the core: In the wall layer, the radial pressure gradient imposed by the high – velocity core is not adequately balance by the local centripetal acceleration. The explanation applies in general terms to secondary flow of Type 1 as well: The direct mixing – stress components generate small cross – channel pressure gradients which can be balance only by a cross – channel of the mean flow.

Type 3 – a component normal to the outer flow in a boundary layer exposed to a pressure gradient which is not parallel to the free stream: Such skewed layers are found near the tips of wing, on swept wing, on the blades of turbomachinery, and at the bottom of a stirred cup of tea, where they are revealed by the motion of the tea leaves.

Type 4 – a boundary layer whose fluid is distorted as the primary flow moves around an obstruction: The vortex lines are stretched by the distortion, and concentrated vortices trail downstream. Complex separating and reattaching flows will be found in the wake and also just ahead of the obstruction. Such flows will occur in the roughness layer near a rough wall, the vortex system around an isolated element taking the form of a househoe vortex wrapped around the protrusion.

Type 5 – the response of a rotating, stratified or electrically conducting fluid when the primary flow is disturbed by an immersed body, by extraction or addition of fluid, or by a change in the rotational speed of a solid boundary.

Type 6: a steady second – order flow associated with a periodic basic flow. Examples are the mean forwards drift associated with waves at the surface of liquid, and the 'acoustic streaming' generated by a body oscillating in air.

Examples of Secondary Flows

a) Tropical cyclones
b) Wind near ground level
c) Tornadoes and dust devils
d) Circular flow in a bowl or cup or Tea leaf paradox
e) River bends
f) Turbomachinery

2.6 Literature Review

Nowadays, a wide range of industries were constructed, many types of fluid, form simple to complex fluid, were used in their processes. Because of the difference in the nature of each fluid, their flow motions are significantly dissimilar especially the flow motion by the complex fluid which are characterized by diverse and often deviations from simple Newtonian behavior. Certainly, in the process industries Newtonian fluids are often the exception rather than the rule. Non-Newtonian fluids are encountered in a vast range of industrial applications, including most multi-phase mixtures (e.g. emulsions, suspensions, foams/froths, dispersions), high molecular weight systems and their solutions (e.g. polymers, proteins, gums), foods, pharmaceuticals, personal care products, agricultural chemicals, synthetic propellants, and slurry fuels. Understanding in their phenomenon is the better way to archive the goal of any engineering exclusively the enigmatic flow which cannot be observe by visual or measure like the secondary flow.

2.6.1 Secondary Flow Appearance in Viscoelastic Fluid and the Effect of Viscoelastic Fluid Parameter on Secondary Flow

Xue et al. [1] used numerical technique to study secondary flows of viscoelastic fluid in straight pipes by an implicit finite volume method based on the SIMPLEST algorithm. The results revealed that the numerical results confirm the theoretical analysis about the existence of secondary flows, and clearly indicate the existence of two counter-rotating vortices in each quadrant of the pipe for all cases, and, with the aspect ratio departing from 1, there is a tendency for the vortex near the long wall to gradually expand and to move to the short wall forcing the vortex near the short wall

to disappear. It is also found that the material parameters have essentially no influence on the pattern of secondary flows, but they strongly affect their strength.

Letelier and Siginer [2] presented the numerical results of the unsteady flow for the Green–Rivlin fluids in arbitrary cross-section straight tubes driven by a pulsating pressure gradient. The results shown that the strength of secondary flows was depended on the values of the physical parameters (ε_1 and n which the parameter ε_1 is intrinsically small, its maximum allowable value decreasing as n increases) associated to each constitutive fluid model. These conditions are replicated in like analysis of other viscoelastic fluids, such as those described by the Phan-Thien–Tanner model, especially for steady flow in non-circular pipes.

Yue et al. [14] studied the mechanism for the secondary flow and developed a general criterion on their direction based on the fluid rheology and the cross-sectional geometry of the pipe. The two main results found that

1. The secondary recirculation was driven by the curl of an effective body force arising from the second normal stress difference (N_2). For this body force to be non-conservative, two conditions have to be satisfied: the rheology must be such that the second normal stress coefficient is not a constant multiple of the shear viscosity, and the cross-section geometry is not axisymmetric.
2. A general criterion on the direction of the secondary flow, based on the ratio between the second normal stress coefficient and the shear viscosity.

Norouzi et al. [15] investigated the inertial and creeping flow of a second-order fluid in a curved duct with a square cross-section and discussed the opposing effects of the first and second normal stress differences. The results revealed that the stability and the intensity of secondary flows was depend on the elastic property of viscoelastic fluid. An increase in the first normal stress difference results in strengthening of the intensity of secondary flows, whereas an increase in the negative second normal difference has the opposite effect. In addition, an increase in the first normal stress difference caused to shift the position of the maximum value of axial velocity to the outer wall, whereas the negative second normal stress difference had the opposite effect.

2.6.2 The Behavior of Newtonian Fluid through Curved Rectangular Micro - channels

Chu at al. [16] investigated the behavior of water through curved rectangular microchannels with different aspect ratios and curvature radii for Reynolds numbers ranging from 10 to 600 by using experimentally-obtained data and numerically-obtained simulation using CFD methodology. The results found that the flow motion in all of experiments are good agreement with the simulation and the predicted by the macro-scale flow theory. The main flow velocity of the inner part of the curved microchannel was lower compared with that of the outer part. However, the velocity distributions of the curved microchannel, which their aspect ratios close to straight were not significantly different from the parabolic profiles of a conventional straight channel flow over the range of De numbers from 2 to 60.

2.6.3 Numerical Methodology based on the Split-Stress Tensor Approach and A New Tool for CFD Simulation of Viscoelastic Fluids

Faveroa et al. [17] presented a new numerical methodology based on the split-stress tensor and the concept of equilibrium stress tensor to treat high Weissenberg number problems using any differential constitutive equations and a new tool for CFD simulation of viscoelastic fluids, the viscoelasticFluidFoam solver.

An extensive testing had shown that a viscoelastic flow solver assembled in this manner works in a stable and efficient manner. Mesh convergence analysis and comparison of the predictions of the viscoelasticFluidFoam solver with the numeric results of Azaiez et al. [18] and the experimental data obtained by Quinzani et al. [19] showed the consistency of the developed tool. Several different constitutive models was tested and the results are in agreement with literature data, confirming that the adopted methodology was successful.

CHAPTER III

SIMULATION

This chapter contains a brief description of the simulation procedure. Simulation works would be separated into four parts; which are

1) Software used
2) Model setup,
3) Investigation of grid independent solutions, and
4) Validation of the model

3.1 Software Used

Three-dimensional simulations were set up and executed using the software OpenFOAM® and ParaView;

3.1.1 OpenFOAM®

The OpenFOAM® (Open Field Operation and Manipulation) CFD Toolbox is a free, open-source CFD software package which developed by OpenCFD Ltd. at ESI Group and distributed by the OpenFOAM Foundation. OpenFOAM has an extensive range of features to solve anything from complex fluid flows involving chemical reactions, turbulence and heat transfer, to solid dynamics and electromagnetics. The core of OpenFOAM is a C++ toolbox that enables the creation of customized numerical solvers. The distribution also contains a wide selection of solvers designed to solve specific problems.

3.1.2 ParaView

This is the main post-processing software distributed with OpenFOAM®. It is an open-source data analysis and visualization tool and it can either be invoked by using paraFoam wrapper script or by converting the data to VTK format and open with ParaView. Data processing can be done either interactively in a 3D environment or using command line batch processing

3.2 Model Setup

3.2.1 Model of the Flow Domain

3.2.1.1 Geometry

In this thesis, the geometries were considered to be the symmetric three-dimensional models with four surface boundaries: inlet, outlet, symmetry, and wall. The models were distinguished into main two parts, including straight and curved conduits. The cross-sectional area and the length of these models are 6.25 cm^2 and 1 m., respectively. The conduit length used was greater than the maximum hydrodynamic entrance length L_h, which was sufficient to obtain a fully developed velocity profile. The six different cross-sectional of conduits, including circle, ellipse, triangle, square, hexagon, and octagon were studied. Geometries of conduit and their informations were shown in Figure 3.1 and Table 3.1, respectively.

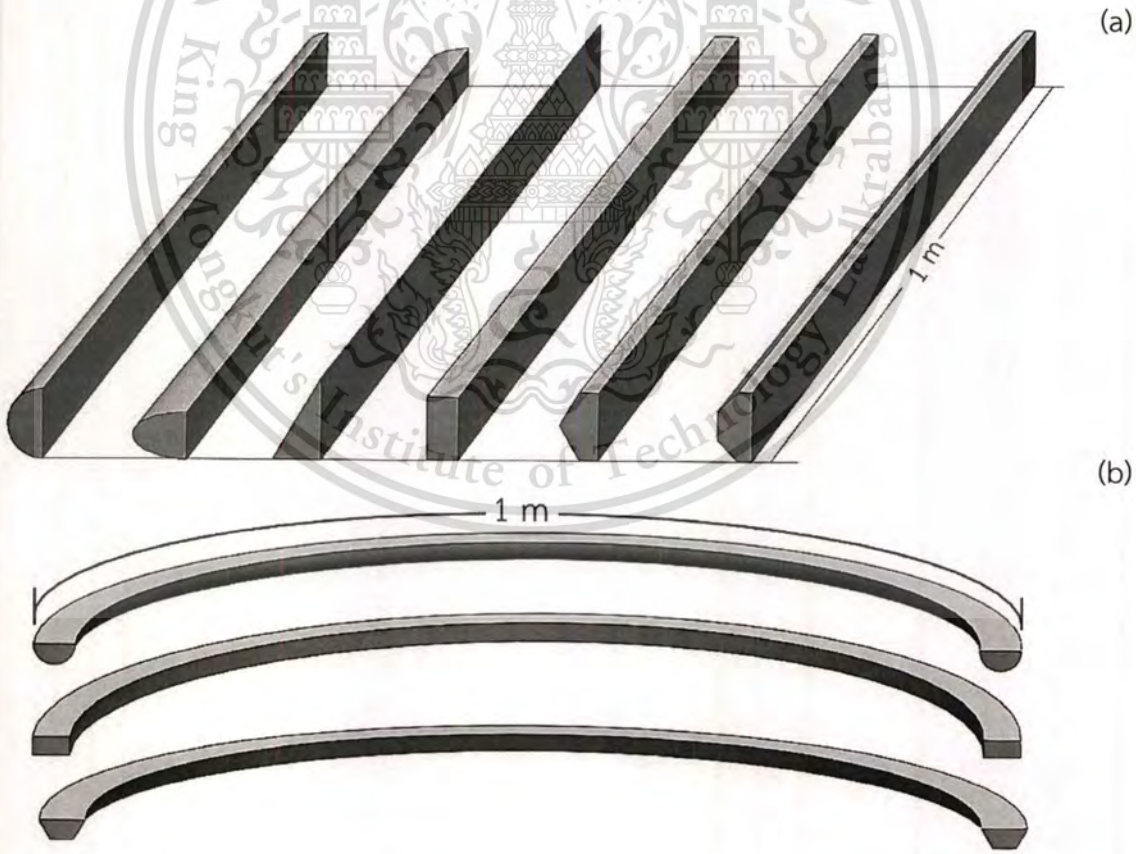

Figure 3.1 The conduit geometries used in this simulation; (a) Straight conduits, (b) some of curved conduits.

Table 3.1 Conduit geometries properties.

Shape	Properties
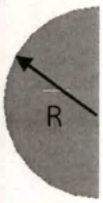	Radiant (R) = 0.0141 m
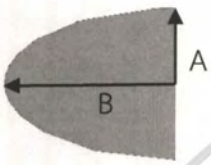	Radiant 1 (A) = 0.0094 m Radiant 2 (B) = 0.0211 m
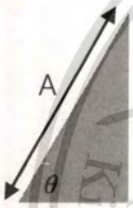	Length of A = 0.0379 m θ = 60 Degree
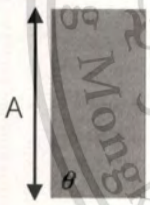	Length of A = 0.025 m θ = 90 Degree
	Length of A = 0.0155 m θ = 30 Degree
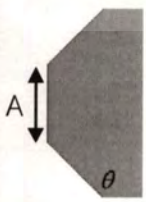	Length of A = 0.0113 m θ = 22.5 Degree

For triangular, hexagonal, and octagonal conduits, their cross – sectional shape are equilateral shape which having all its sides of the same length as same as the square.

3.2.1.2 Mesh

A structured mesh with hexahedra grid cells was generated for simulate the flows. To optimize the mesh size it was necessary to carry out a mesh-independence study; this was done by performing a number of simulations with different mesh sizes, starting from a coarse mesh and refining it until results were no longer dependent on the mesh size.

For all of 3-D mesh size, the high refinement of mesh near the wall were designed to enhance mesh resolution in this region where high velocity and shear stress exist. The refinement contained twenty inflation layers which the first layer has a thickness of 0.01 mm and expanded by a factor of 1.2 in successive layers. The example of this refinement is shown in Figure 3.2.

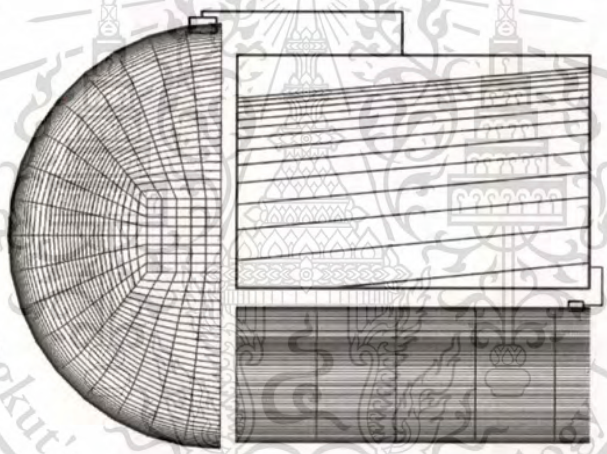

Figure 3.2 The example of the refinement of mesh applied on the conduit.

3.2.2 Boundary Conditions

The boundary conditions were applied to four surface boundaries; inlet, outlet, symmetry, and wall, as shown in Figure 3.3, in which the details of each surface as the following;

a) The fluid inlet was assumed to be uniform with the different velocity magnitude depend on fluid type and cross-sectional shape.

b) A no-slip wall boundary condition was applied at the pipe wall.

c) The symmetry boundary condition was adopted at the conduit symmetric centerline.

d) The zero velocity derivative and zero pressure were used at conduit outlet.

e) For viscoelastic fluid, the zero stress tensor was used at the inlet for the conduit. In addition, zero gradient condition was applied for the other remaining boundaries.

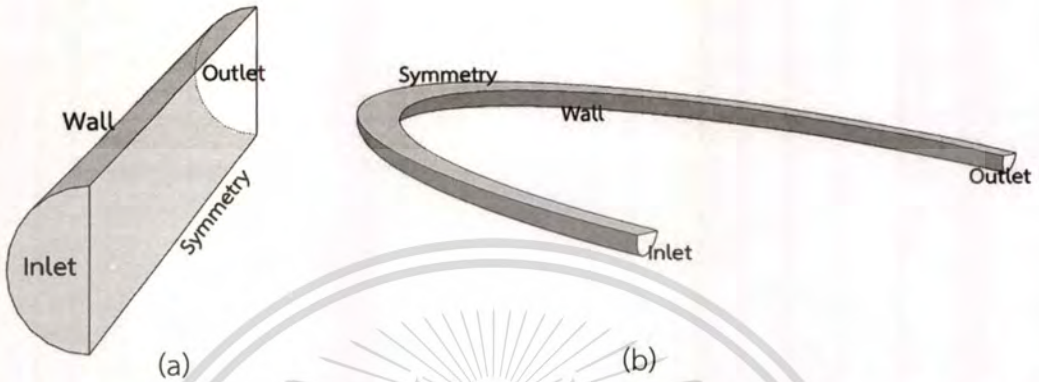

Figure 3.3 The example of boundary conditions in circular conduit, (a) Straight, (b) Curved.

3.2.3 Assumptions of the Model

In this simulation, the assumption of the model can be described as the following;

1) The flow domains were symmetric three – dimensional model which the symmetry boundary condition was applied at the conduit symmetric centerline to reduce a number of mesh and computational effort in problem. At this boundary condition, zero normal velocity and zero normal gradients of all variables were assumed.
2) Fluids were considered to be isothermal and incompressible.
3) The Fluid motion was assumed to be laminar flow.

3.2.4 Governing Equations of the Model

According to the assumptions of the model, the governing equations of the model, including continuity equation, momentum equations, and constitutive equations for viscoelastic fluid can be expressed below.

The isothermal incompressible flows of Newtonian and viscoelastic fluids were considered to be three-dimensional laminar flow. Both of the flow systems were governed by mass and momentum conservation equations that can be written in the following form.

Mass conservation equation:

$$\nabla \cdot \mathbf{u} = 0 \tag{3.1}$$

Momentum conservation equation:

$$\frac{\partial(\rho \mathbf{u})}{\partial t} + \nabla \cdot (\rho \mathbf{u}\mathbf{u}) = -\nabla p + \nabla \cdot \boldsymbol{\tau} + S_M \tag{3.2}$$

For viscoelastic fluid, a constitutive equation was added into the momentum equation to describe the relation between the stress and deformation rate. The stress tensor of viscoelastic fluid in the above equation can be divided into two contributions, a Newtonian solvent contribution $\boldsymbol{\tau}_S$ and an elastic polymeric contribution (or extra elastic stress tensor) $\boldsymbol{\tau}_P$, as shown in equation (3).

$$\boldsymbol{\tau} = \boldsymbol{\tau}_S + \boldsymbol{\tau}_P \tag{3.3}$$

with $\boldsymbol{\tau}_s$ was defined by:

$$\boldsymbol{\tau}_S = 2\eta_S \mathbf{D} \tag{3.4}$$

where $\mathbf{D}$ is the deformation rate tensor given by:

$$\mathbf{D} = \frac{1}{2}\left(\nabla \mathbf{u} + [\nabla \mathbf{u}]^{\mathrm{T}}\right) \tag{3.5}$$

and $\boldsymbol{\tau}_P$ was obtained as the sum of the contributions of the individual relaxation modes:

$$\boldsymbol{\tau}_P = \sum_{K=1}^{n} \boldsymbol{\tau}_{P_K} \tag{3.6}$$

with the expression for $\boldsymbol{\tau}_{P_K}$ depending on the viscoelastic constitutive equation.

The Giesekus constitutive equation was used in the simulations. The model is based on a kinetic theory of closely packed polymer chains and a series of simplifications leading to an equation for the extra stress that contains no explicit integrals over the configurations of individual molecules. The extra stress for the Giesekus model is given by:

$$\boldsymbol{\tau}_{P_K} + \lambda \overset{\nabla}{\boldsymbol{\tau}}_{P_K} + \alpha_K \frac{\lambda_K}{\eta_P}\left(\boldsymbol{\tau}_{P_K} \cdot \boldsymbol{\tau}_{P_K}\right) = 2\eta_{P_K}\mathbf{D} \tag{3.7}$$

where $\overset{\nabla}{\boldsymbol{\tau}}_{P_K}$ is the expressions for the upper-convected time derivative of the individual relaxation modes which can be specified by the following equation:

$$\overset{\nabla}{\boldsymbol{\tau}}_{P_K} = \frac{D}{Dt}\boldsymbol{\tau}_{P_K} - \left[\nabla \mathbf{u}^T \cdot \boldsymbol{\tau}_{P_K}\right] - \left[\boldsymbol{\tau}_{P_K} \cdot \nabla \mathbf{u}\right] \tag{3.8}$$

The parameters used for single-mode Giesekus model are shown in Table 3.2.

Table 3.2 Parameters of the single-mode Giesekus constitutive equation.

α	$\lambda(\mathrm{s})$	$\eta_P(\mathrm{Pa\,s})$	$\eta_S(\mathrm{Pa\,s})$
0.15	0.03	1.422	0.002

3.2.5 Numerical Methods

The governing equations have been solved numerically by OpenFOAM® with the PISO algorithm (Pressure Implicit with Splitting of Operators) which is an efficient method to solve the Navier-Stokes equations in unsteady problems. By using of the finite volume method (FVM), the computation domain is divided into a number of small cells, and the partial differential equations are integrated over the flow domain to obtain a set of algebraic equations. These algebraic equations were solved iteratively to obtain the field distribution of dependent variables. For this study, the resulting linear discretized systems were solved by conjugated gradient method (CG) as detailed in Table 3.3. The absolute tolerance for pressure was 1.0×10^{-7} and for velocity and stress was 1.0×10^{-6}.

Table 3.3 The resulting linear discretized systems for pressure, velocity, and stress.

Parameter	Discretized Systems	Precondition
Pressure	Preconditioned Conjugate Gradient Method	Diagonal Incomplete – Cholesky Method
Velocity and Stress	Preconditioned Bi-Conjugate Gradient Method	Diagonal Incomplete Lower-Upper Method

3.3 Validation of the Simulation Model

Validation can defined as a process for assessing simulation modeling uncertainty by using benchmark experimental data [20]. The velocity profile of Newtonian laminar flow in circular conduit and the properties of viscoelastic fluid, were validated by comparing with the theory and the simulated results which reported by J.L. Favero [17], respectively.

3.4 Parameters of the Simulation

The Parameters of this simulation were distinguish as the following;

3.4.1 Newtonian Fluid and Viscoelastic Fluid Properties

The Newtonian and viscoelastic fluids in this simulation were water (ρ = 998.21 kg/m^3 , μ = 1.002 $Pa \cdot s$) and a polymer solution of 5wt. % of Poly-isobutylene (PIB) in Tetradecane (C14) (ρ = 803.87 kg/m^3), respectively.

3.4.2 Effect of Conduit Shape

The effect of the conduit shape was investigated by different conduit shapes, including circle, ellipse, triangle, square, hexagon, and octagon. The inlet velocities for each conduit are different depend on their shape (hydraulic diameter) and fluid type. The inlet velocities are shown in Table 3.4.

Table 3.4 Cross-sectional shape and the velocity magnitude ($\mathbf{Re}$ = 5) of each models.

Shape	Velocity magnitude (m/s)
	$V_{Newtonian} = 1.78 \times 10^{-4}$ $V_{Viscoelastic} = 3.14 \times 10^{-1}$
	$V_{Newtonian} = 2.29 \times 10^{-4}$ $V_{Viscoelastic} = 3.53 \times 10^{-1}$
	$V_{Newtonian} = 2.29 \times 10^{-4}$ $V_{Viscoelastic} = 4.04 \times 10^{-1}$

Table 3.4 Cross-sectional shape and the velocity magnitude ($\mathbf{Re}$ = 5) of each models.

Shape	Velocity magnitude (m/s)
	$V_{Newtonian} = 2.01 \times 10^{-4}$ $V_{Viscoelastic} = 3.54 \times 10^{-1}$
	$V_{Newtonian} = 1.87 \times 10^{-4}$ $V_{Viscoelastic} = 3.30 \times 10^{-1}$
	$V_{Newtonian} = 1.83 \times 10^{-4}$ $V_{Viscoelastic} = 3.22 \times 10^{-1}$

where $V_{Newtonian}$ and $V_{Viscoelastic}$ are the inlet velocity of Newtonian fluid and viscoelastic fluid, respectively.

To make a clearly understanding in the effect of conduit shape, the square was chosen and then, transform its shape to be the circular by adding roundness to it corners as shown in Figure 3.4. The degree of roundness and velocities are shown in Table 3.5.

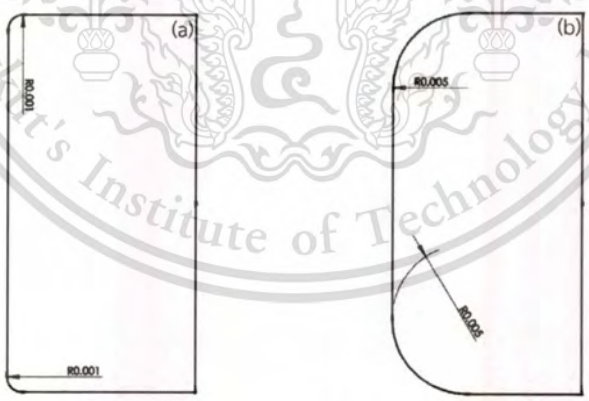

Figure 3.4 The example of square conduit with added roundness; (a) 0.1 cm, (b) 0.5 cm.

Table 3.5 The degree of roundness and velocities magnitude ($\mathbf{Re}$ = 5) of each models.

Roundness	Velocity magnitude (m/s)
R = 0.0005 	$V_{Newtonian} = 1.99 \times 10^{-4}$ $V_{Viscoelastic} = 3.51 \times 10^{-1}$

Table 3.5 (Cont.) The degree of roundness and velocities magnitude ($\mathbf{Re}$ = 5) of each models.

Roundness	Velocity magnitude (m/s)
R = 0.0010 	$V_{Newtonian} = 1.98 \times 10^{-4}$ $V_{Viscoelastic} = 3.48 \times 10^{-1}$
R = 0.0025 	$V_{Newtonian} = 1.93 \times 10^{-4}$ $V_{Viscoelastic} = 3.41 \times 10^{-1}$
R = 0.0050 	$V_{Newtonian} = 1.87 \times 10^{-4}$ $V_{Viscoelastic} = 3.30 \times 10^{-1}$
R = 0.0075 	$V_{Newtonian} = 1.83 \times 10^{-4}$ $V_{Viscoelastic} = 3.22 \times 10^{-1}$
R = 0.0100 	$V_{Newtonian} = 1.80 \times 10^{-4}$ $V_{Viscoelastic} = 3.17 \times 10^{-1}$

3.4.3 Effect of Bending and Bended Shape Orientations

The effect of the bending and their orientations were investigated under the identical condition in the straight conduits except for the triangular conduit shape (type 1) which was created in full shape conduit because its shape not symmetry when it was bended. Conduits were bended with radius = 0.318 m, which give the same length of conduit when it was straight as shown in Figure 3.5. The bended conduit shape orientations are shown in Table 3.6.

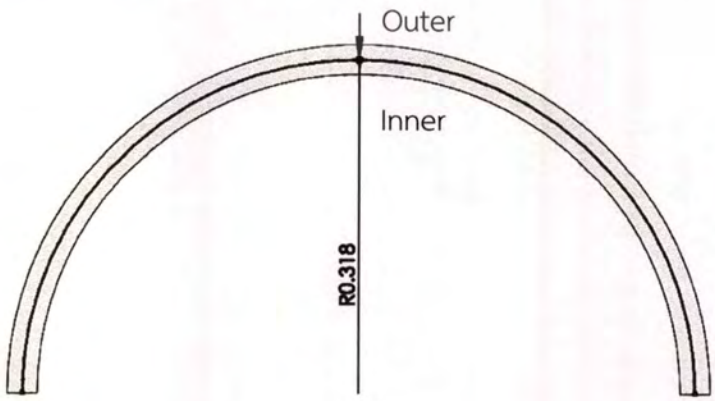

Figure 3.5 The conduit bending degree.

Table 3.6 The bended conduit shape orientations.

Shape	Orientation (type)
	Outer  Inner
	Outer  Type 1  Type 2 Inner
	Outer  Type 1  Type 2  Type 3 Inner
	Outer  Type 1 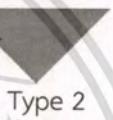 Type 2 Inner
	Outer  Type 1  Type 2 Inner
	Outer  Type 1  Type 2 Inner

3.4.4 Effect of Inlet Velocity

The effect of velocity was investigated by ranging Reynolds numbers from 5 – 200. The square conduits was chosen as test geometry. The added velocity magnitude for each Reynolds numbers and each type of fluid are shown in Table 3.7.

Table 3.7 The variation of velocity magnitude.

Reynolds Number	Velocity Magnitude (m/s)	
	Newtonian Fluid	Viscoelastic Fluid
10	4.02×10^{-4}	0.71
50	2.01×10^{-3}	3.54
100	4.02×10^{-3}	7.09
200	8.04×10^{-3}	14.20

CHAPTER IV

RESULTS AND DISCUSSION

4.1 Mesh Independence Study

In this part, the circular conduit was only modeled to examine mesh independent study. All of various mesh sizes are consisted of same high refinement mesh near wall. The geometry was distinguished into three parts by mesh generation, including high refinement zone (A) as described in 3.2.1.2 , outer zone (B), and inner zone (C), which was created for generating hexahedra mesh cells, as shown in Figure 4.1(a).

The initial mesh size was generated and controlled by dividing conduit perimeter and parts of conduit diameter (outer zone) into small section which the initial section of divided perimeter is 12 sections and the initial section of divided part of conduit diameter is 14 sections, respectively. The initial mesh along conduit length was started by dividing conduit length into 30 sections. The initial mesh size is shown in Figure 4.1(b)

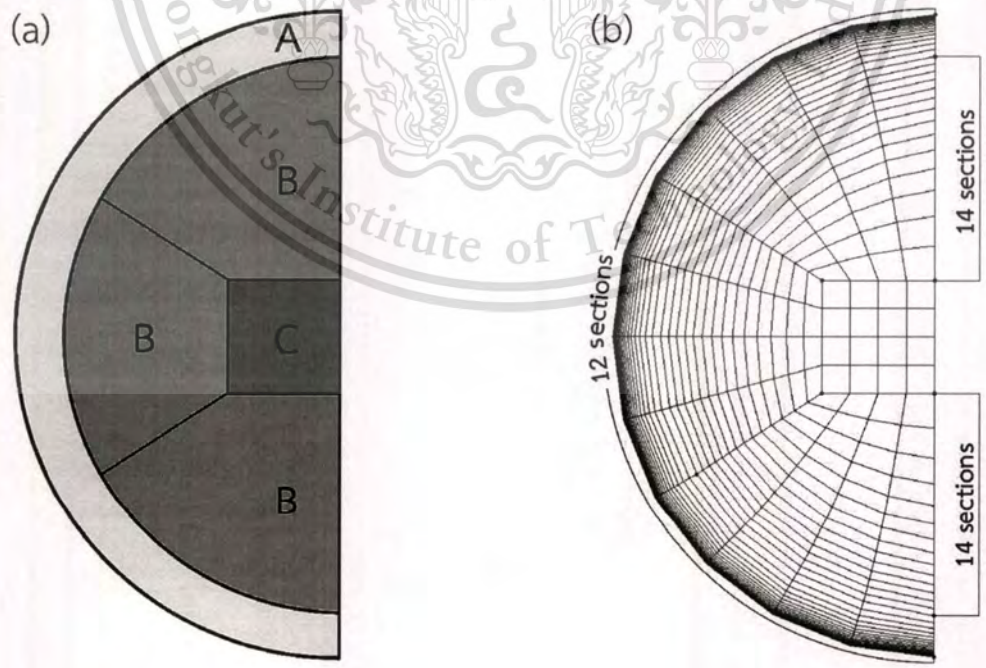

Figure 4.1 The geometry of the model; (a) zone, and (b) the initial mesh size.

To determine the mesh independent, Number of sections in the initial mesh size was multiplied by 1.5, 2, and 2.5. The various mesh size form coarse to fine mesh are shown in Figure 4.2. The information of mesh quality and mesh quantity is shown in Table 4.1.

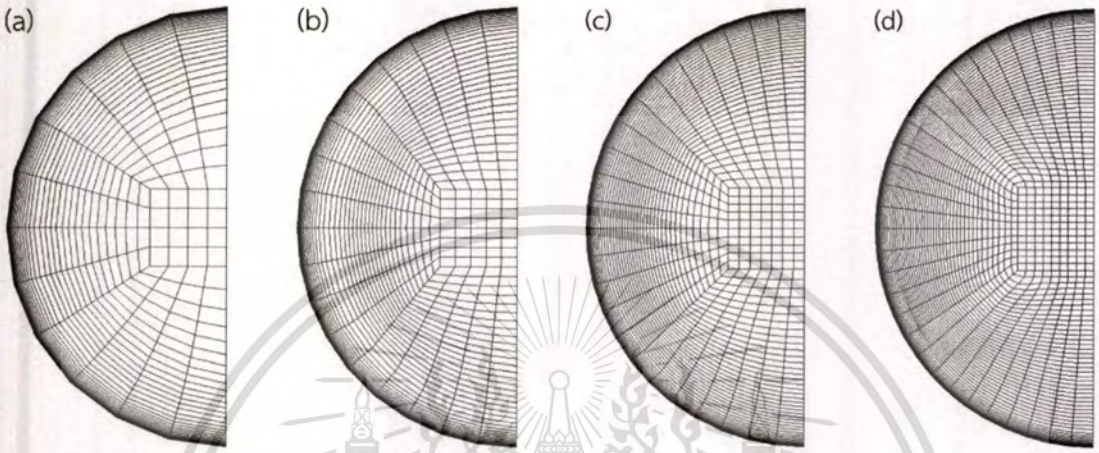

Figure 4.2 Mesh generation of the model and mesh size varied from; (a) 1 (the initial mesh size), (b) 1.5, (c) 2, and (d) 2.5.

Table 4.1 The information of different mesh size.

Factors	Mesh Quality		Mesh Quantity
	Non- orthogonality	Max. aspect ratio	Number of cells
1 (The Initial size)	Max: 27.86 Average: 3.29	3,292.98 (on 2,280 cells)	12,720
1.5	Max: 34.84 Average: 5.59	2,204.02 (on 3,330 cells)	35,010
2	Max: 36.38 Average: 5.40	1,656.02 (on 3,840 cells)	69,000
2.5	Max: 35.66 Average: 6.78	1,326.37 (on 3,300 cells)	122,850

The simulated data were compared when the values of interest (pressure and velocity) have reached a steady solution (after 40 minute for both of fluid type) as shown in Figure 4.3.

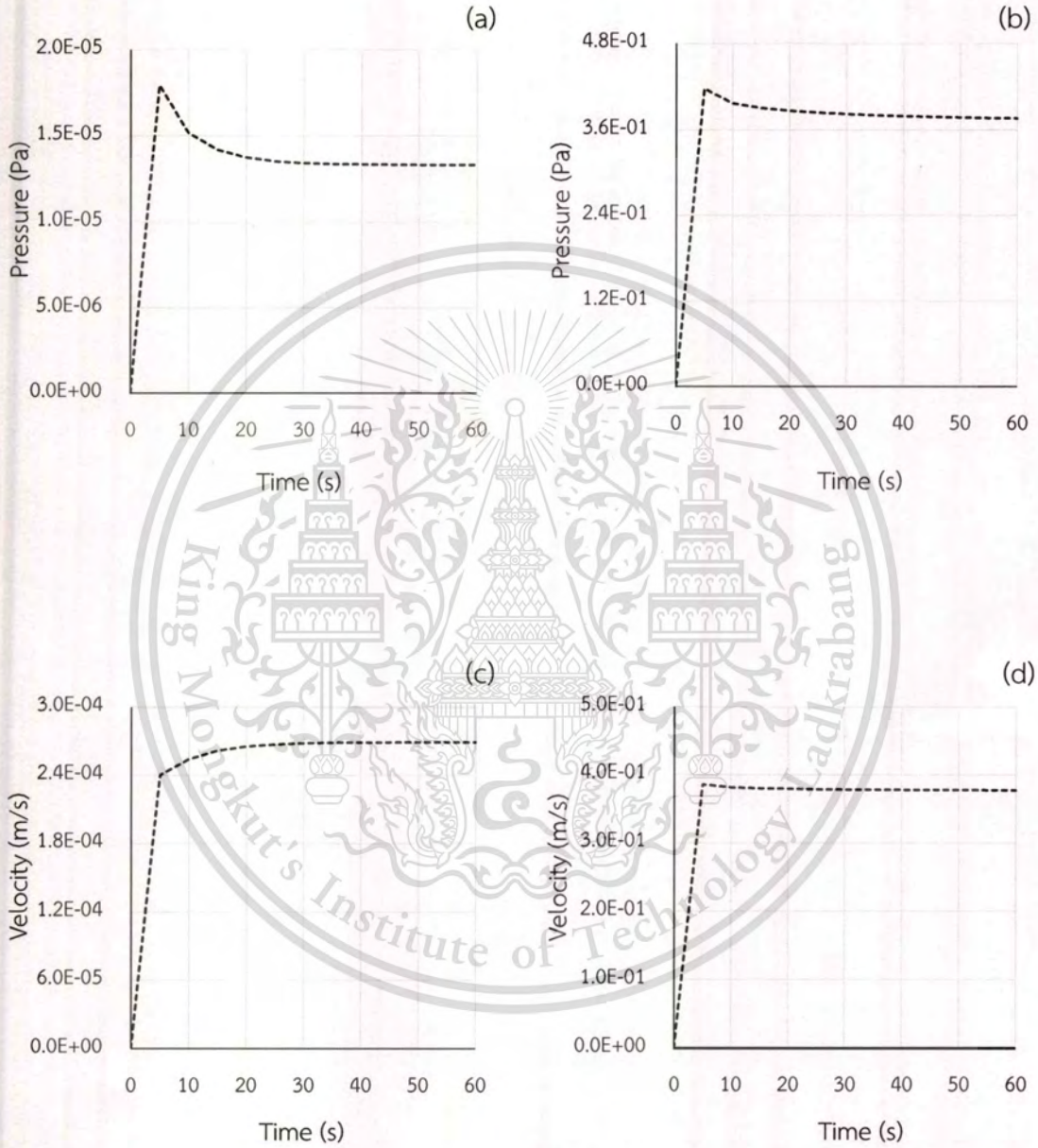

Figure 4.3 A steady state solutions for this simulation; (a) Pressure for Newtonian fluid, (b) Pressure for viscoelastic fluid, (c) Velocity for Newtonian fluid, and (d) Velocity for viscoelastic fluid.

The simulation results showed that mesh independent study was obtained at number of mesh cells equal to 35,010 (The initial mesh size multiply by 1.5) as shown in Figure 4.4.

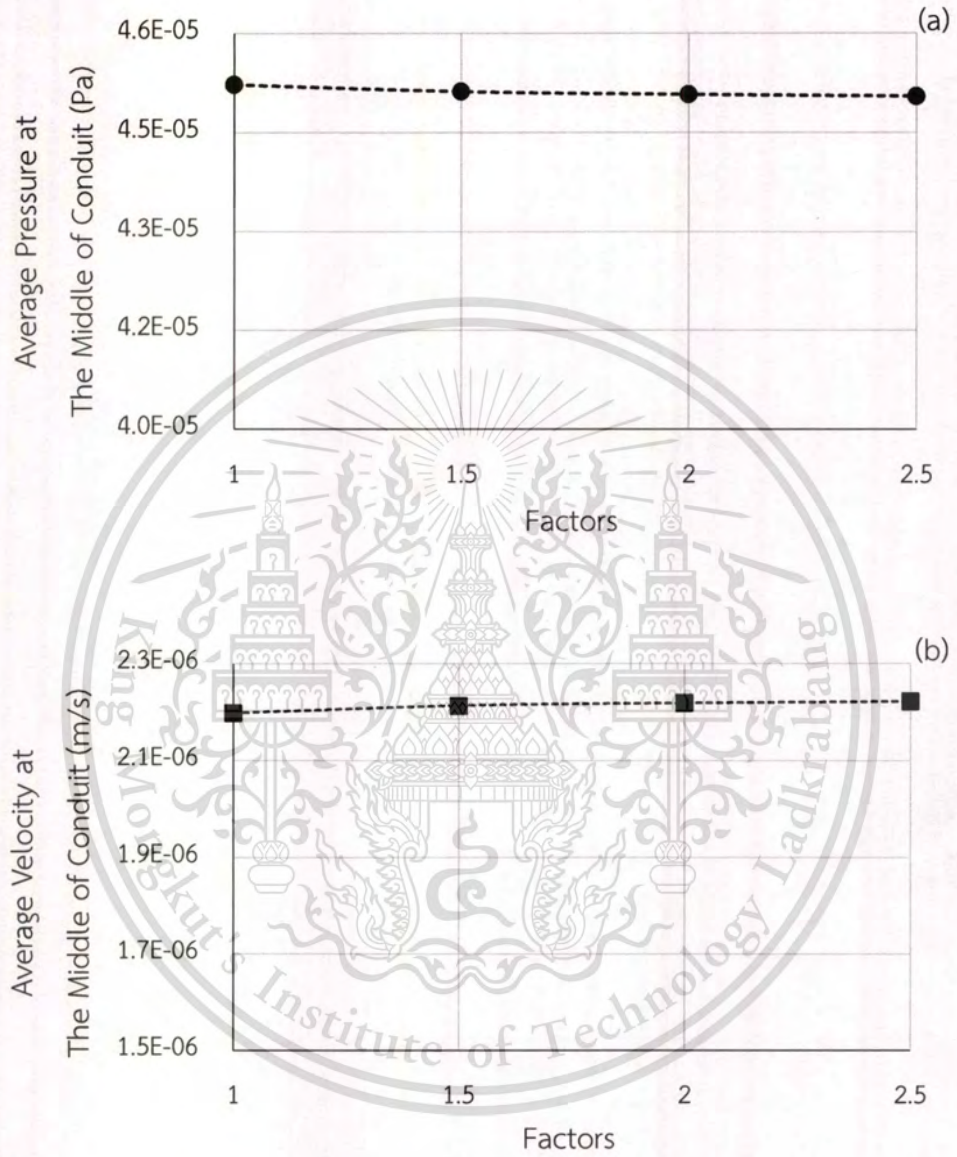

Figure 4.4 The simulated data with different number of mesh cells; (a) The average pressure at the middle of conduits, and (b) The average velocity at the middle of conduits.

According to mesh independent study, the other models were generated with mesh size of the initial mash size multiply by 1.5 and increase the results of simulation along conduit length by using mesh size multiply by 2 (60 sections).

4.2 Validation of the model

4.2.1 Validation of the Flow Model

Validation of the steady state solution of the model was carried out by comparing CFD predictions of the velocity field and the total volumetric flow rate through the pipe with the exact analytical solutions obtained by theory. As will be shown below, CFD is generally capable of yielding very accurate predictions of the steady laminar flow in pipes. The simulated results were collected from the middle of the conduit which its length was also greater than the maximum hydrodynamic entrance length L_h.

4.2.1.1 Flow rate

The exact value of flow rate which given by cross – sectional area of the conduit multiplied with the inlet velocity, was compared with the calculated flow rate from maximum velocity which give by CFD simulation through the Pouiseuille equation (Equation 4.1). The percentage error shown in Table 4.2 is calculated by Equation 4.2

$$Q = \frac{\pi R^2 v_c}{2} = \frac{\pi D^4 \Delta p}{128 \mu l} \tag{4.1}$$

where $R, v_c, \Delta p, \mu$, and l are conduit radius, maximum velocity, pressure drop, fluid viscosity, and conduit length, respectively.

$$\text{The persentage eror} = \left| \frac{Q_{\text{CFD}} - Q_{\text{Exact}}}{Q_{\text{Exact}}} \times 100 \right| \tag{4.2}$$

Table 4.2 Comparison between the volumetric flow rates by calculated from maximum velocity (CFD result) and exact value.

Exact value (m^3/s)	Calculated from CFD result (m^3/s)	Error (%)
1.113×10^{-7}	1.107×10^{-7}	0.54

4.2.1.2 Velocity profile

The velocity profile obtained by CFD was compared with the theoretical velocity profile which calculated from the relation of the Pouiseuille equation (Equation 4.1) and equation 4.3.

$$u(r) = \frac{\Delta p D^2}{16 \mu l}\left[1 - \left(\frac{2r}{D}\right)^2\right] \tag{4.3}$$

The comparison between the theoretical velocity profile and velocity profile obtained by CFD simulation was shown as Figure 4.5.

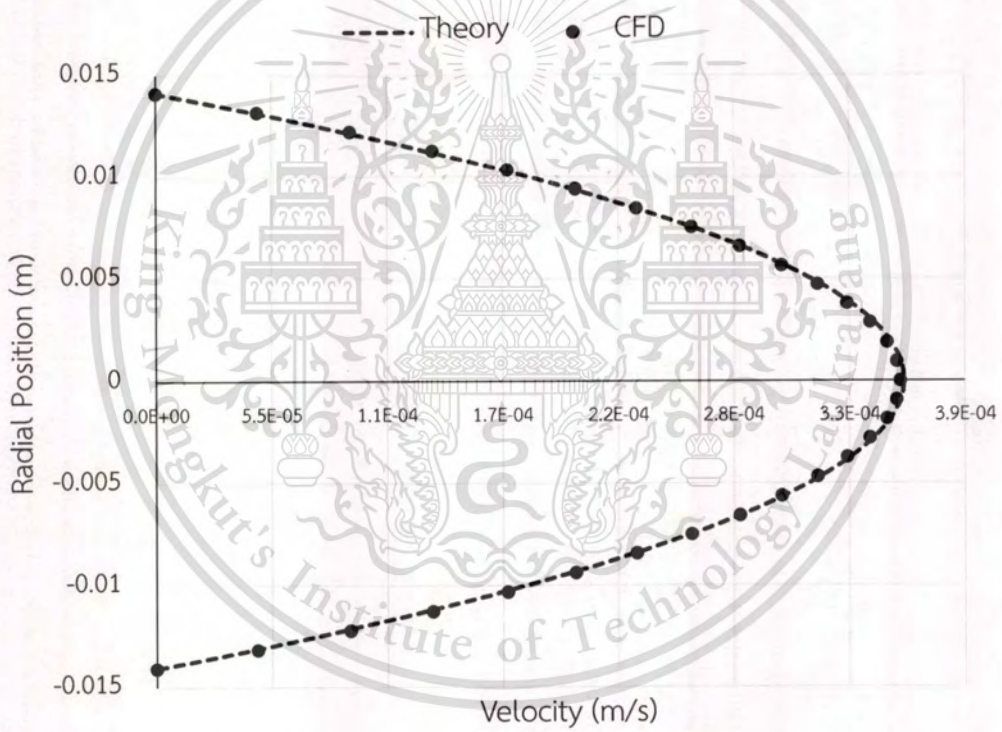

Figure 4.5 Comparison of CFD-predicted and theoretical velocity profiles.

4.2.2 Validation *of Viscoelastic Fluid Properties*

In order to verify the properties of viscoelastic fluid, a planar abrupt contraction with contraction ratio H/h of 3.97 (upstream thickness of 2H (0.0254 m) and downstream thickness of 2h (0.0064 m)), as depicted in Figure 4.6, was chosen as a test geometry because of the availability of previous CFD simulation by J.L. Favero [17].

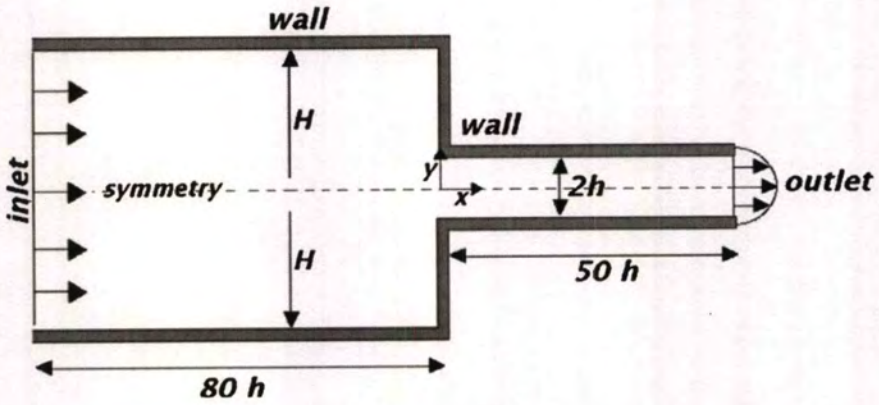

Figure 4.6 Test geometry for verify the properties of viscoelastic fluid.

The simulated results were validated by comparing with the previous simulation data. The comparison between the simulated vertical velocity and the previous data were in acceptable level with the error of 0.56% as shown in Figure 4.7.

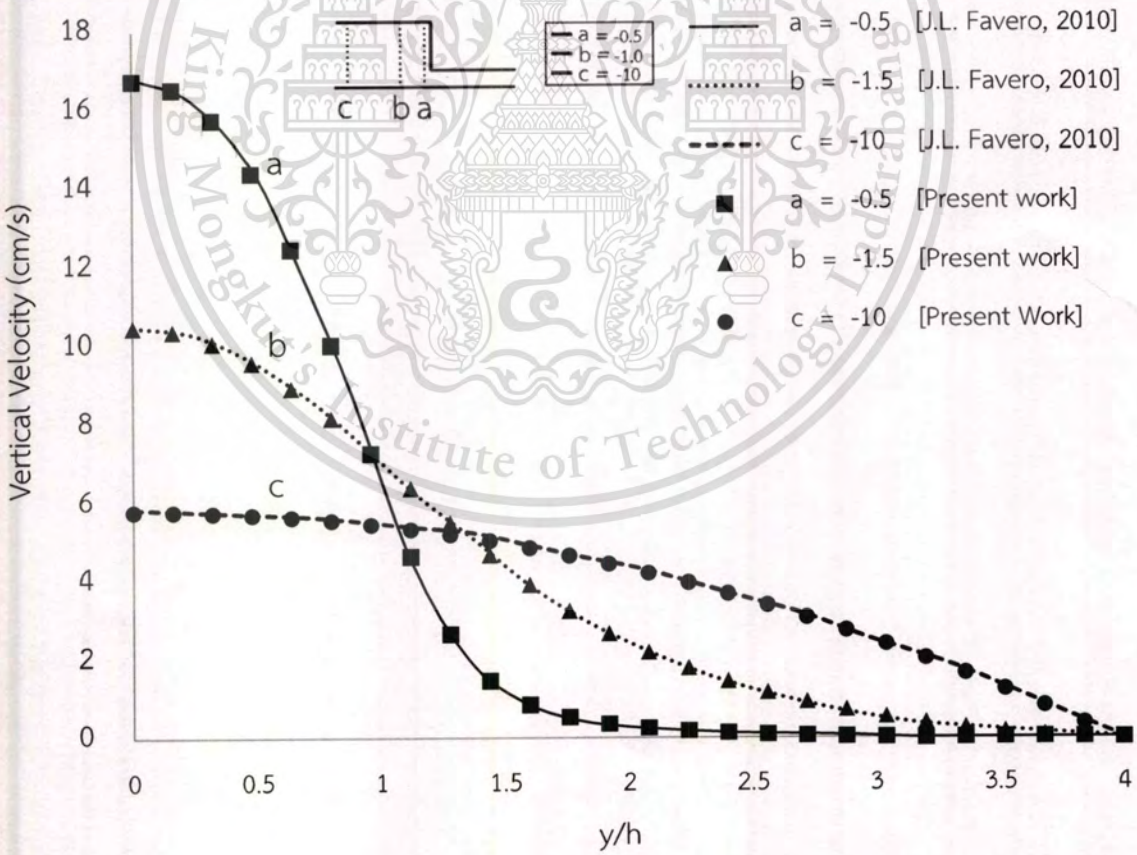

Figure 4.7 The comparison between the simulated vertical velocity profiles and the previous data.

4.3 The Secondary Flow in various shape conduits and flow conditions

In this part, the investigation of this simulation was distinguished into three part including;

1) The effect of conduit geometry (Newtonian fluid)
2) The effect of velocity inlet (Newtonian fluid)
3) The effect of fluid type

The results in the first and the second part were discussed only on the phenomena that occurred in Newtonian fluid. However, both of effects which impact on Viscoelastic fluid were reported and discussed in the third part, instead.

4.3.1 Effect of Conduit Geometry

4.3.1.1 Effect of conduit shape

The simulation of Newtonian fluid flow for six various shaped conduits including circle, ellipse, triangle, square, hexagon, and octagon were studied with Reynolds number of 5 and measured the desired properties at the middle of the conduits.

Friction velocity ($\mathbf{u}_f$), defined by

$$\mathbf{u}_f \equiv \left(\frac{\tau_w}{\rho}\right)^{\frac{1}{2}} \tag{4.4}$$

was chosen as a reference velocity to compare secondary flows strength in each case because both of compared variable ($\mathbf{u}_f$ and $\mathbf{u}_{secondary}$) had significant effect in the same range of region which close to the wall.

The simulated results revealed that the laminar secondary flow of Newtonian fluid was slightly occurred. Their strength ($(\mathbf{u}_{secondary}/\mathbf{u}_f)\times 100$) were in the range of 0.0005 – 0.0054% which the lowest value was given by the circular shape (rarely occurred). The increasing of conduit angle give the higher of secondary flow strength which reach the highest value by the square shape and then this value was dropped as shown in Table 4.3 and Figure 4.8 which showed the secondary flow velocity magnitude of each conduit.

Table 4.3 The strength of secondary flow in various shaped conduits.

Conduit shape	The strength of secondary flow (%)
Circular	0.0005
Elliptic	0.0016
Triangular	0.0036
Square	0.0054
Hexagonal	0.0044
Octagonal	0.0006

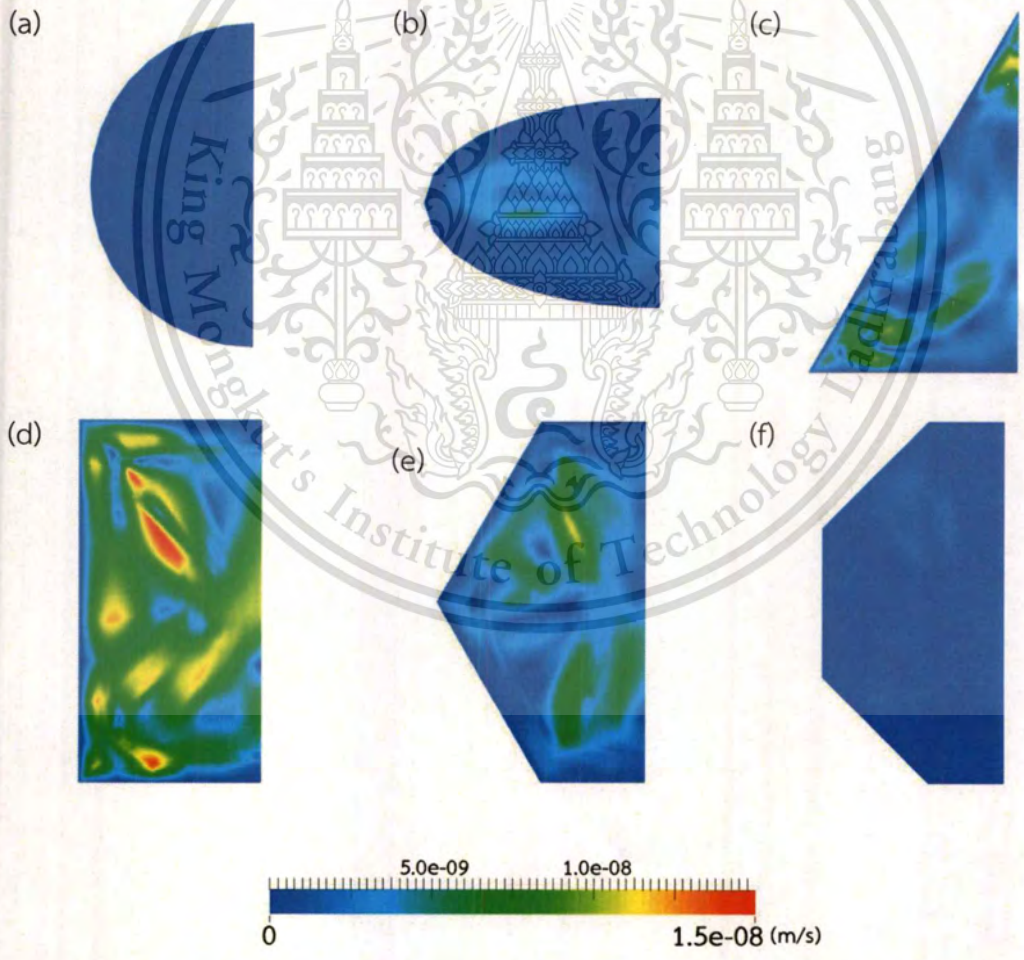

Figure 4.8 Velocity contour of secondary flow in various shaped conduit; (a) circular, (b) elliptic, (c) triangular, (d) square, (e) hexagonal, and (f) octagonal shape conduit.

The secondary flow patterns were comprised of the stochastic vortices which were depended on the cross-sectional area of conduit as shown in Figure 4.9.

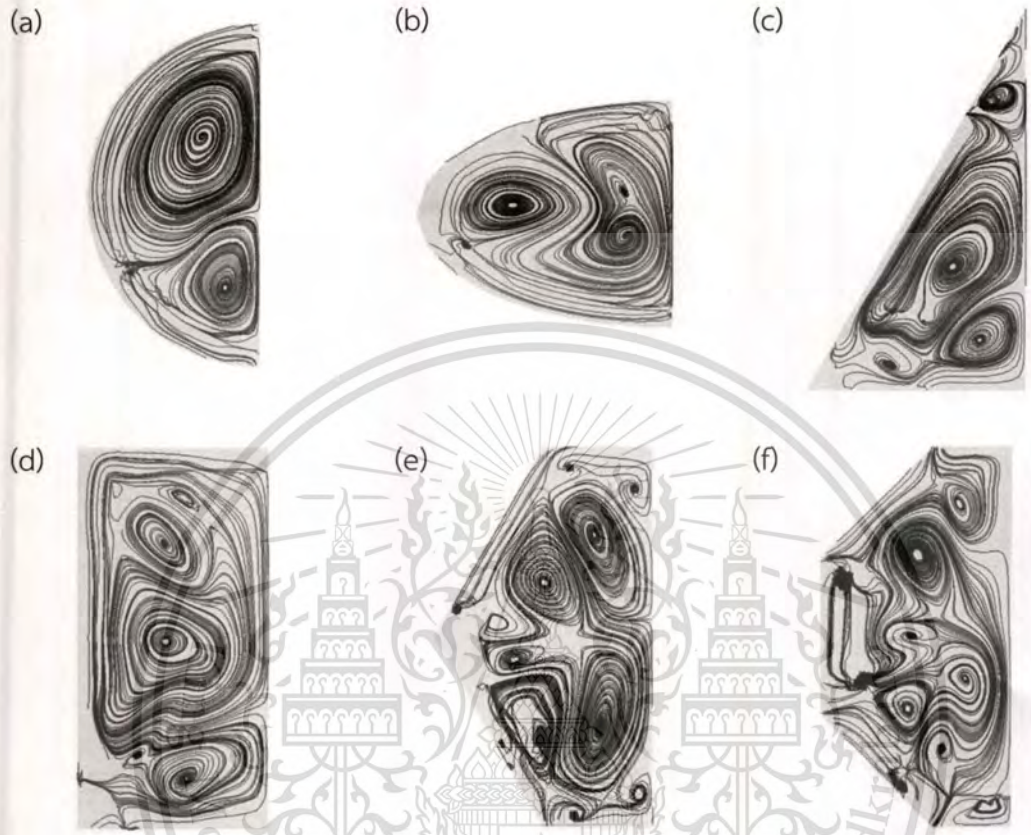

Figure 4.9 Streamline of secondary flow in various shaped conduit; (a) circular, (b) elliptic, (c) triangular, (d) square, (e) hexagonal, and (f) octagonal shape conduit.

From the simulated results, the secondary flow in the non-circular conduits were stronger than in the circular. These results corresponded to the literature [13] which explain this phenomena by the unbalance of direct shear stresses.

This unbalance was occurred in non-axisymmetric conduit more than in another as shown in Figure 4.10 which showed the wall shear stress of various conduit shape along their perimeter. This increasing of the unbalance required more strength of secondary flow to generate cross-stream shear stresses for stabilizing the variations in direct stresses [13].

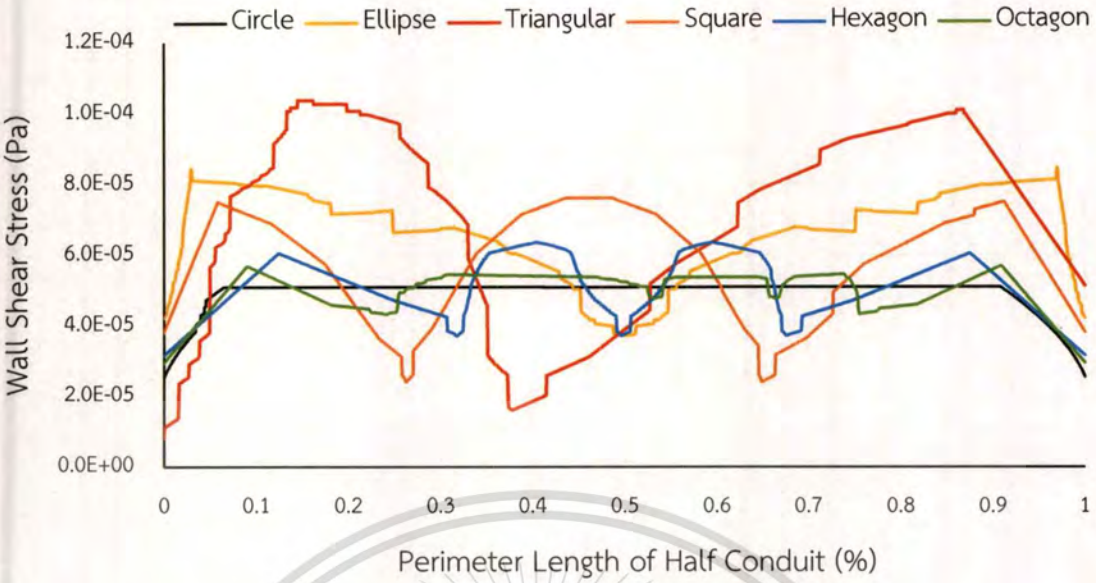

Figure 4.10 The simulated wall shear stress profile in each half conduit shapes.

From Figure 4.10, the unbalance of direct stress was increased when conduits had more number of angle and then this unbalance was decreased after it reach the highest value which given by the triangular geometry. The mechanism that cause this phenomena is the generation of vertices by conduit corner for stabilizing the unbalance of direct stress instead of the increasing of the secondary flow strength as shown by their streamline. However, Newtonian fluid produced very small value of secondary flow velocity magnitude which cause the order of secondary flow strength was not correspond to the unbalance that occurred by the different of conduit geometries.

To make a clearly understanding in this effect, the flow motion through round corners conduits were simulated. The square conduit was chosen as a test geometry. The roundness of the corner were varied in the range of 0.05 – 1.00 cm.

Table 4.4 showed the strength of secondary flow in conduit with various degrees of corner roundness. The velocity profile and streamline of secondary flow in various degrees of corner roundness are shown in Figure 4.11 and Figure 4.12, respectively.

The simulated results revealed that the velocity magnitude and the strength of secondary flow decreased when the roundness was added. The unbalance of direct stress in sharp corner conduit was stabilized by adding the roundness as show in Figure 4.13

Table 4.4 The strength of secondary flow in various degree of corner roundness.

The degree of corner roundness	The strength of secondary flow (%)
0.0000 (Square conduit)	0.0054
0.0005	0.0012
0.0010	0.0005
0.0025	0.0007
0.0050	0.0003
0.0075	0.0004
0.0100	0.0006
0.0141 (Circular conduit)	0.0005

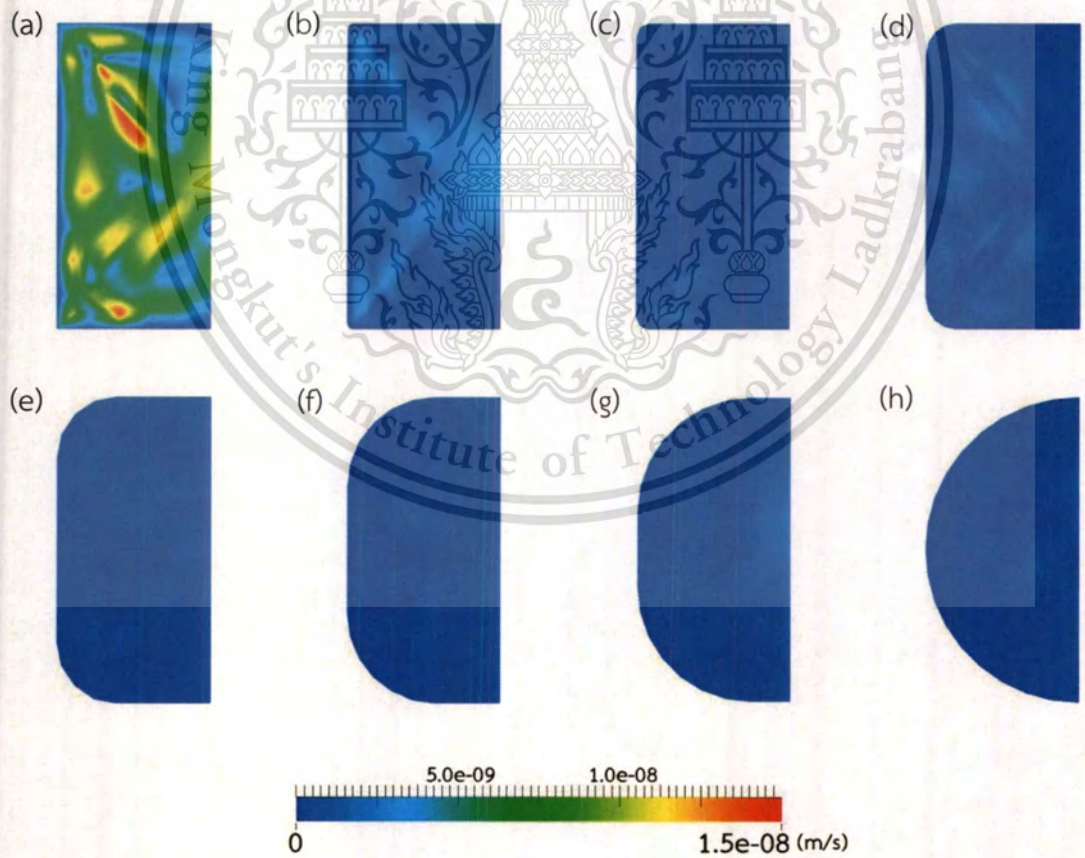

Figure 4.11 Velocity contour of secondary flow in various degree of corner roundness; (a) 0, (b) 0.0005, (c) 0.001, (d) 0.0025, (e) 0.005, (f) 0.0075, (g) 0.01, and (h) 0.0141.

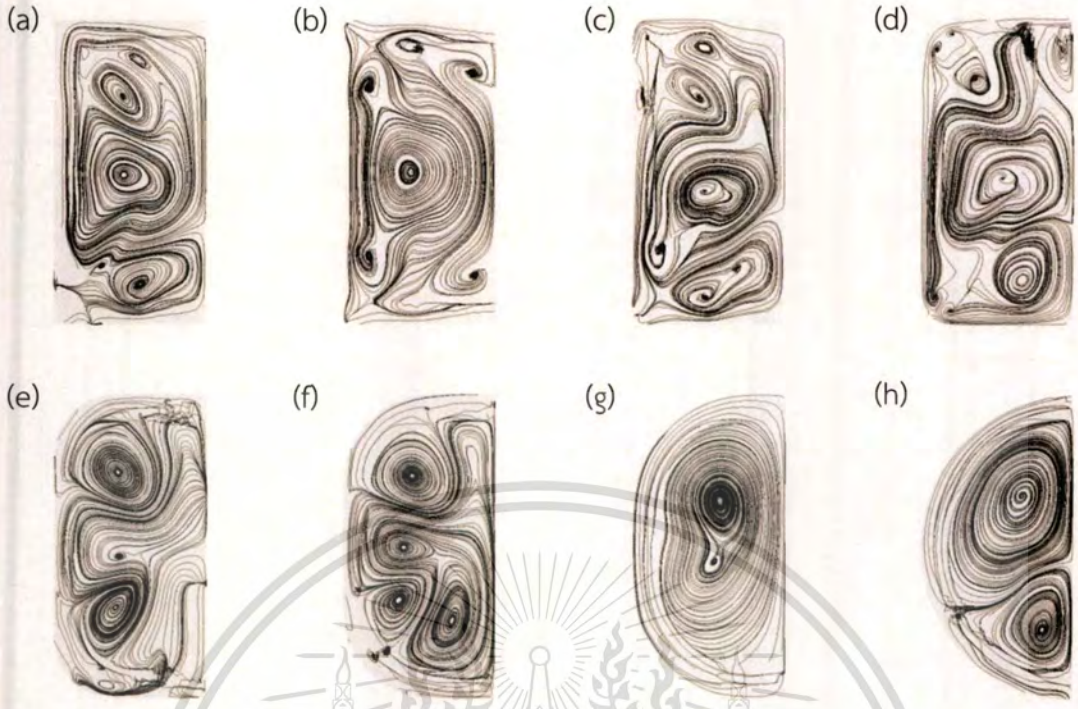

Figure 4.12 Streamline of secondary flow in various degree of corner roundness; (a) 0, (b) 0.0005, (c) 0.001, (d) 0.0025, (e) 0.005, (f) 0.0075, (g) 0.01, and (h) 0.0141.

Figure 4.13 showed the simulated wall shear stress profile in half conduits with the difference in degree of corner roundness

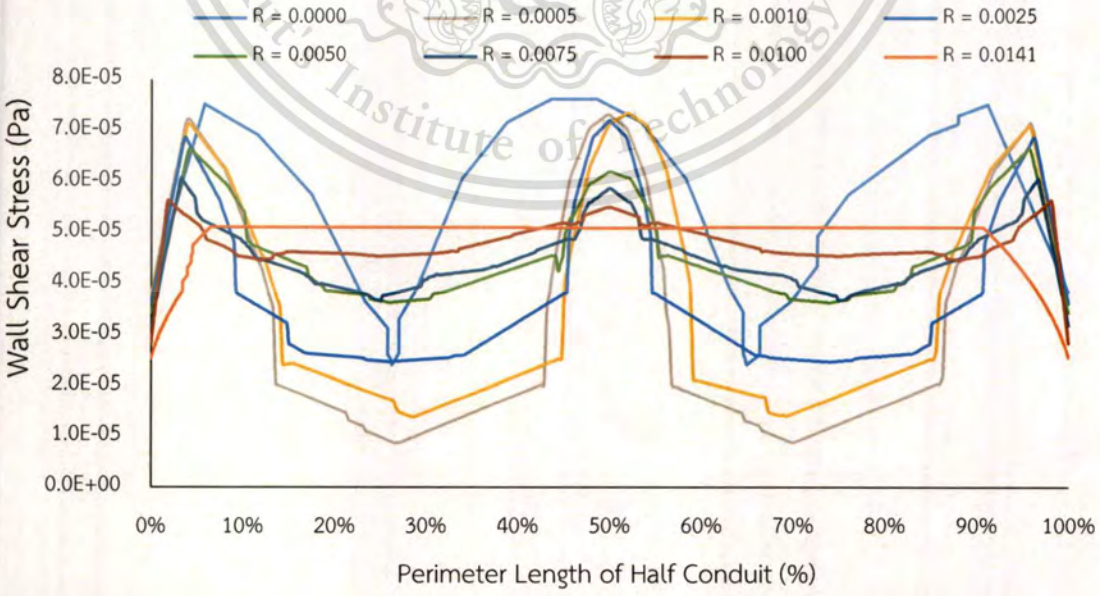

Figure 4.13 The simulated wall shear stress profile in half conduit with the difference in degree of corner roundness.

4.3.1.2 Effect of bending and bended shape orientations

4.3.1.2.1 Effect of bending

The various curved shaped conduits were studied under the identical condition in the straight conduits.

From the simulated results, bending produced the pressure gradient across the cross-sectional area in each conduit as illustrated the example in Figure 4.14 and 4.15.

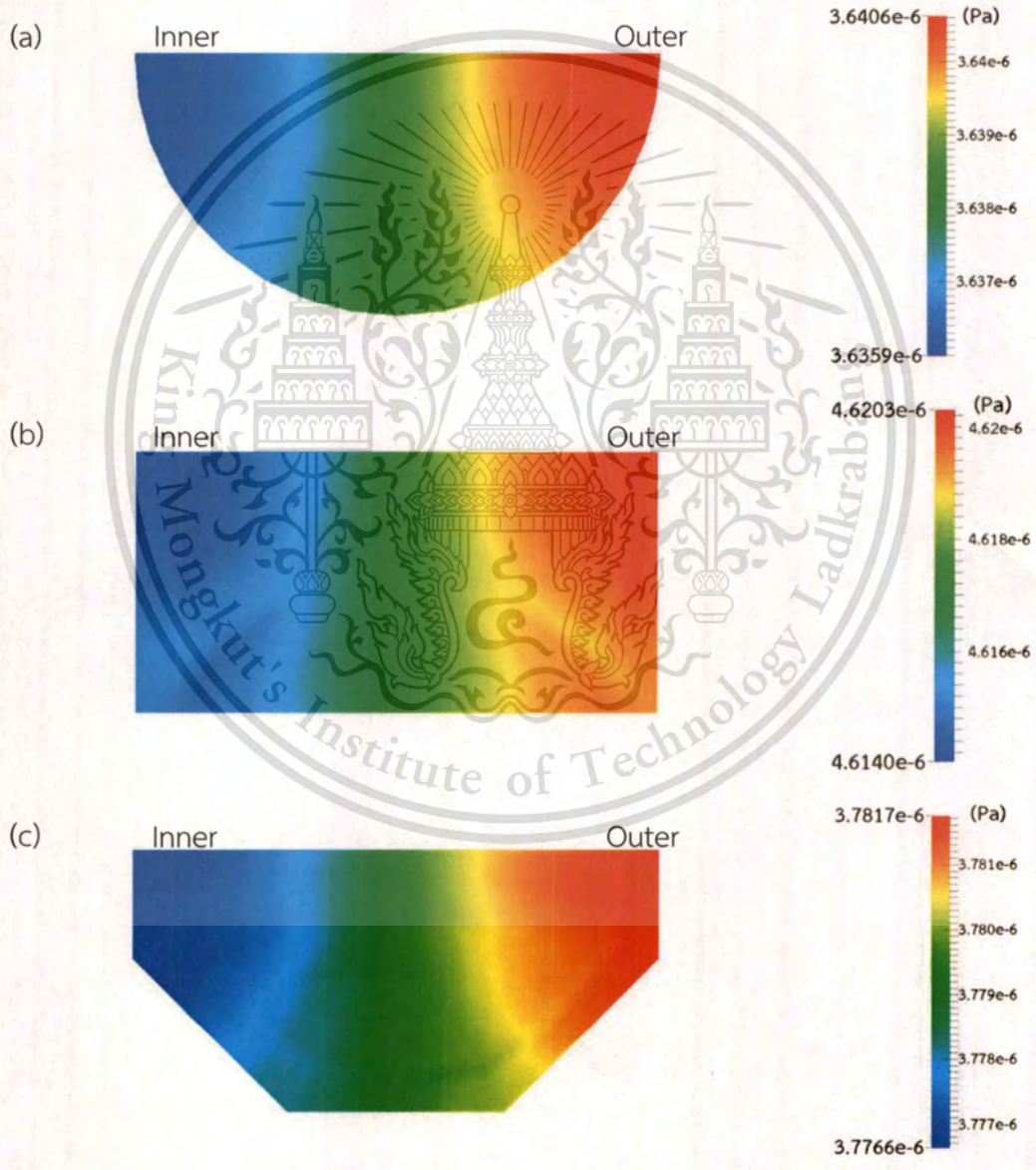

Figure 4.14 The pressure contour that occurred between the inner and the outer side of various curved conduit; (a) circular, (b) square, and (c) octagonal shape conduit.

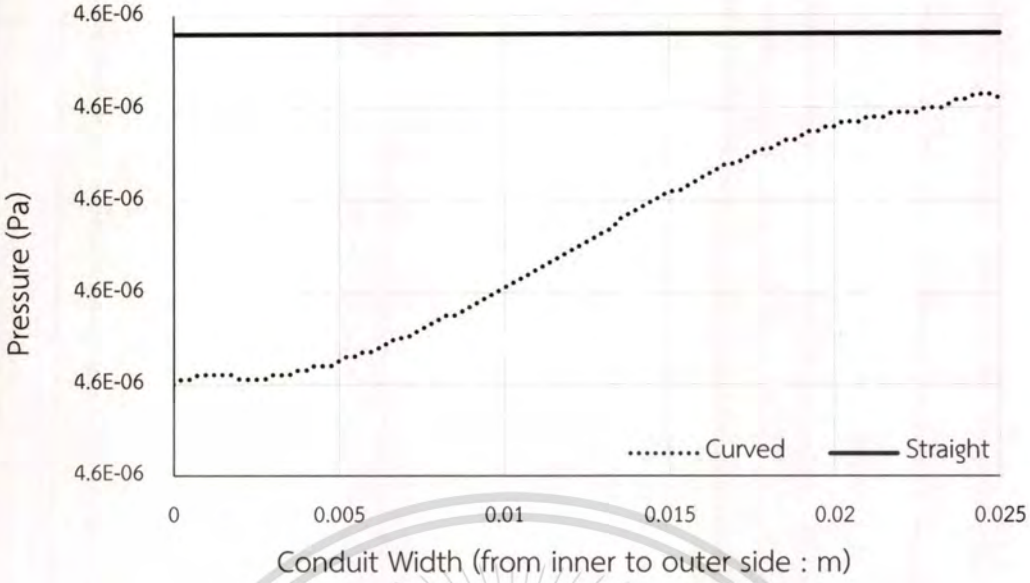

Figure 4.15 Pressure gradient at the center of the conduit between the inner and the outer side of square conduit.

The pressure gradient was significantly affected on secondary flows as an addition of the unbalance in direct shear stresses between the inner and outer side of the conduit as the example which shown in Table 4.5. This gradient also bring the change of secondary flow pattern and their magnitude.

Table 4.5 The mean shear stress at the center of the square conduit.

Conduit type	Inner Side (Pa)	Outer Side (Pa)	The Difference (Pa)
Straight	6.07×10^{-5}	6.07×10^{-5}	0.00
Curved	5.74×10^{-5}	6.02×10^{-5}	2.79×10^{-6}

The pattern of secondary flow in each curved conduit was quite similar. The observation of this pattern was made up of two-vortex flow which rotate in the opposite direction in the upper and the lower part of the conduit as shown in Figure 4.16. This change found to increase the magnitude and the strength of secondary about 99 % and 0.4 – 0.5 %, respectively. In addition, the added unbalance of direct shear stress cause least impact on the difference of conduit shape as shown in Table 4.6.

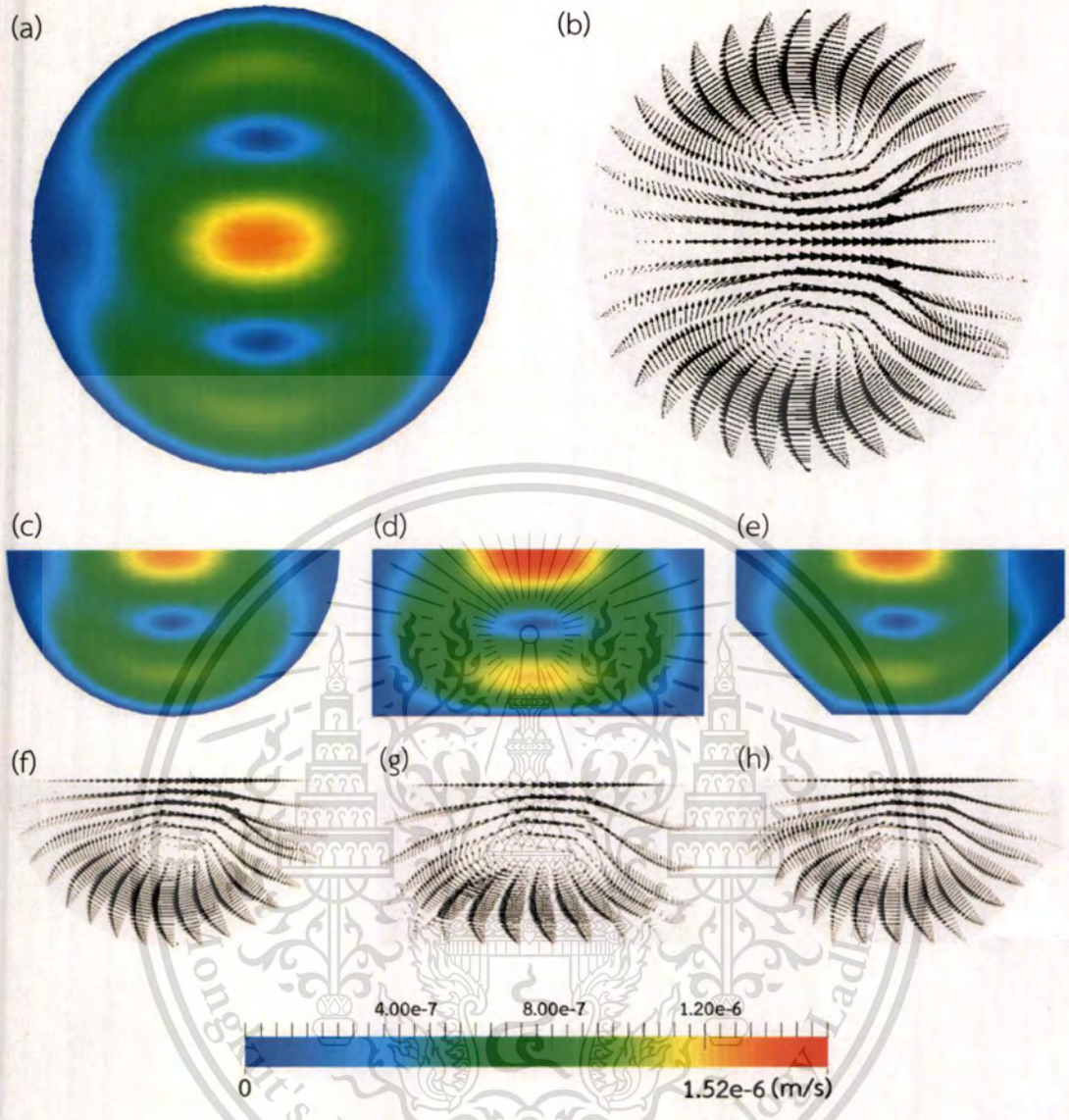

Figure 4.16 The velocity magnitude contour and vector profile of secondary flow in various curved conduits; (a) full circular contour, (b) full circular vector, (c) half circular contour, (d) half square contour, (e) half octagonal contour, (f) half circular vector, (g) half square vector, and (h) half octagonal vector profile.

Table 4.6 The velocity magnitude and strength of secondary flow in curved conduits.

Conduit shape	Velocity magnitude (m/s)	Strength (%)
Circular	1.03×10^{-6}	0.449
Elliptic	8.81×10^{-7}	0.302

Table 4.6 (Cont.) The velocity magnitude and strength of secondary flow in curved conduits.

Conduit shape	Velocity magnitude (m/s)	Strength (%)
Triangular	1.47×10^{-6}	0.453
Square	1.20×10^{-6}	0.434
Hexagonal	1.06×10^{-6}	0.417
Octagonal	1.08×10^{-6}	0.441

4.3.1.2.2 Effect of bended shape orientations

When the conduits were bended, some of conduit shape can be placed into the different layout. Bended conduit by setting more number of angle to the outer side of the curved gave the higher value of secondary flow strength because the unbalance of direct shear stress can be more produced when the flow motion associated with the angle of conduit as shown in Figure 4.17. However, this effect have no significant impact to the secondary flow, compare with the pressure gradient that occurred by the bending. The strength of secondary flow by changing conduit orientations are shown in Table 4.7.

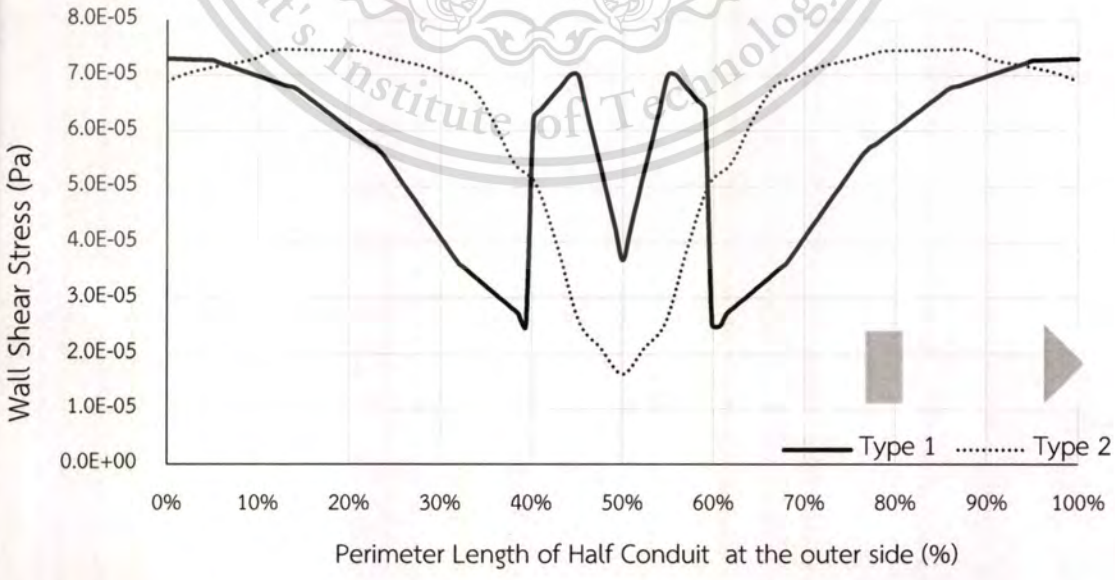

Figure 4.17 The simulated wall shear stress profile at the outer side of square conduit with two different geometry layout.

Table 4.7 The strength of secondary flow by changing conduit orientations.

Conduit shape	Type	Secondary flow strength (%)
Elliptic	1	0.302
	2	0.214
Triangular	1	0.453
	2	0.471
	3	0.464
Square	1	0.434
	2	0.455
Hexagonal	1	0.417
	2	0.443
Octagonal	1	0.441
	2	0.437

4.3.2 Effect of Inlet Velocity

In this part, the square conduit was chosen as a test geometry to investigate the effect of inlet velocity. The various velocities, which varies by Reynolds number from 5 to 200, were studied in both of straight and curved conduit.

The simulated results found that the secondary flow strength in straight conduit is proportional to the increasing of inlet velocity as shown in Figure 4.18.

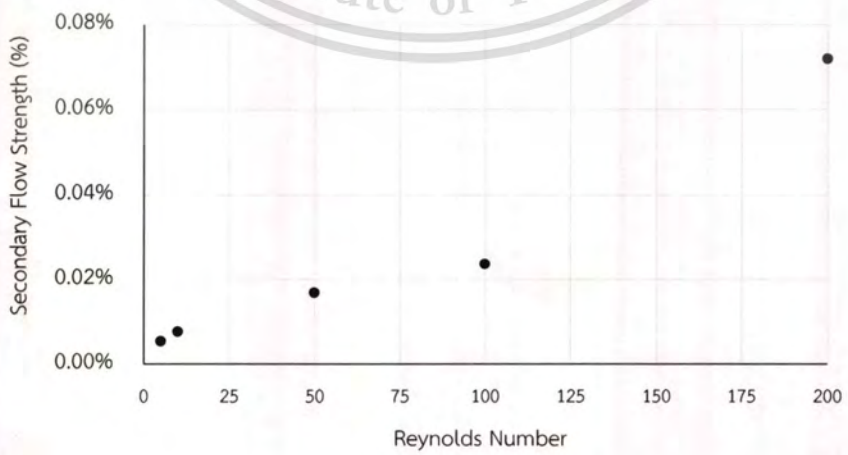

Figure 4.18 The secondary flow strength in straight square conduits by various Reynolds number.

At mention earlier, the secondary flow pattern in straight conduit at lower Reynolds number (**Re** = 5) was comprised of the stochastic vortices. However, this vortices became orderly pattern, which the variation of velocities in cross-stream were induced to the center of the conduit, when Reynolds number was higher as shown in Figure 4.19 and Figure 4.20.

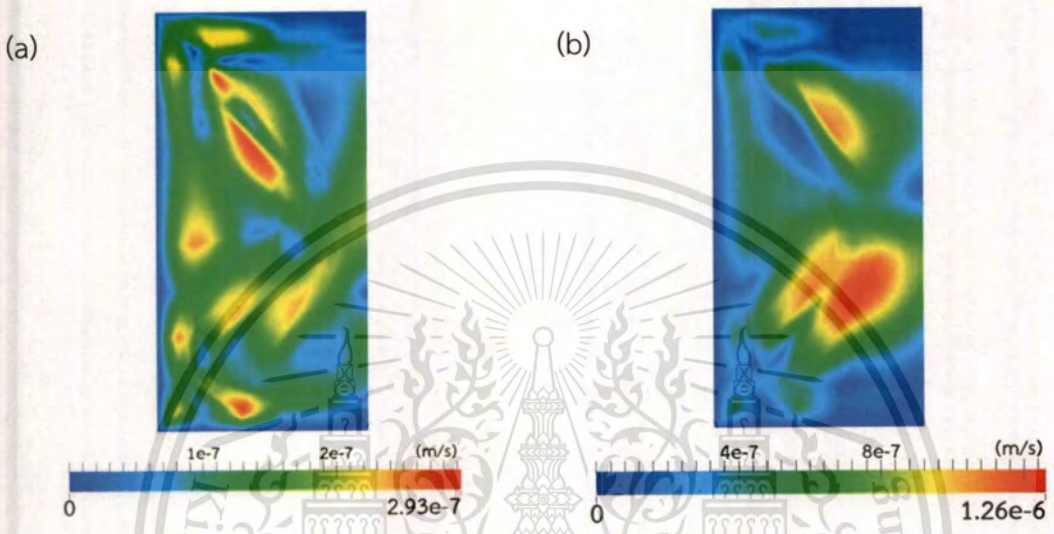

Figure 4.19 The secondary flow contour of lower Reynolds number (**Re** = 100) and higher Reynolds number (**Re** = 200) in square conduit; (a) **Re** = 100, and (b) **Re** = 100.

Figure 4.20 The secondary flow vector profile of lower Reynolds number (**Re** = 100) and higher Reynolds number (**Re** = 200) in square conduit; (a) **Re** = 100, and (b) **Re** = 100.

For curved conduit, the results was different from the straight. The strength of secondary flow instantly increased at first, then decreased after the pattern of secondary flow was changed. However, the strength of secondary flow also increased by higher Reynolds number after this decreasing as shown in Figure 4.21. The cause of this decreasing was more effect of the velocity which was induced into the core flow.

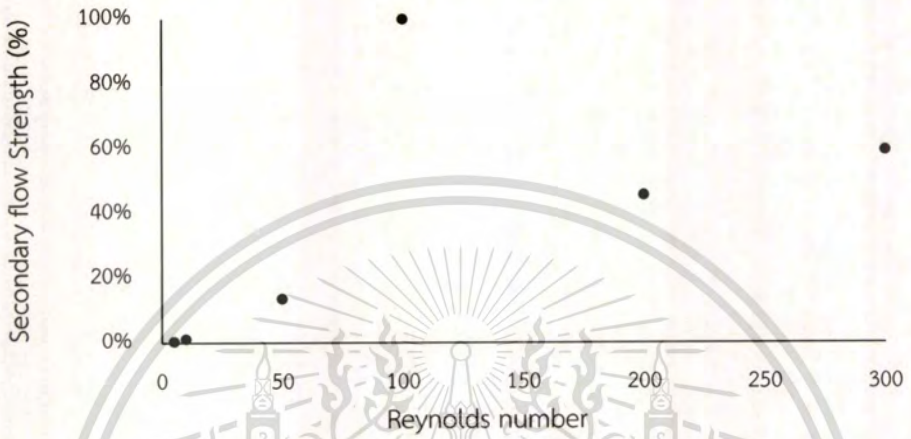

Figure 4.21 The secondary flow strength in curved square conduits by various Reynolds number.

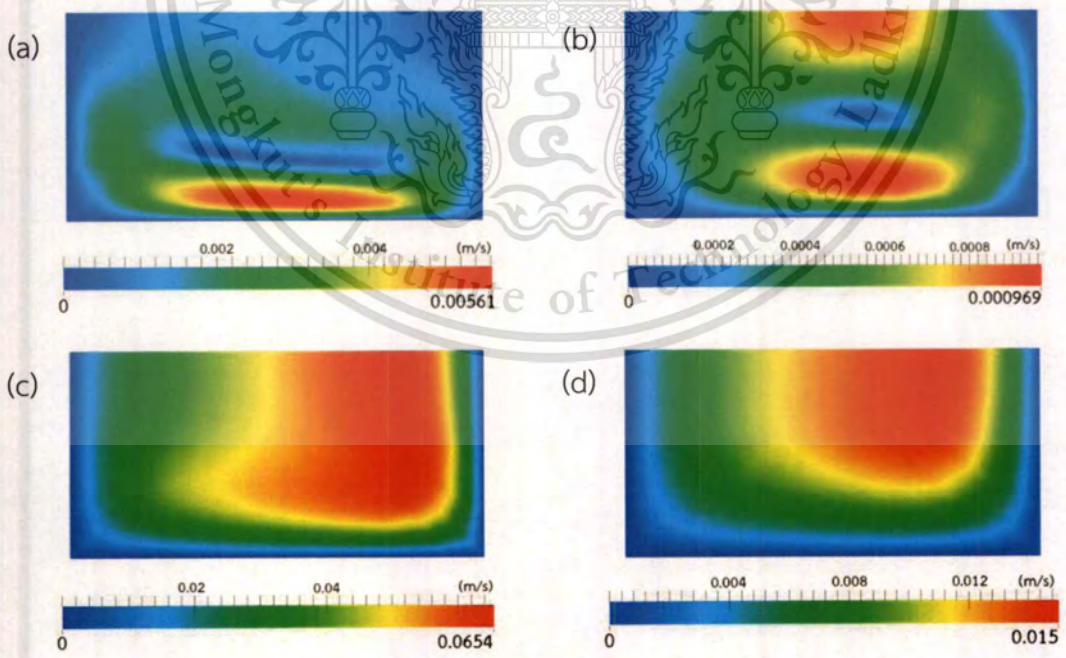

Figure 4.22 The secondary flow and primary velocity contour of lower Reynolds number ($\mathbf{Re}$ = 100) and higher Reynolds number ($\mathbf{Re}$ = 200) in curved square conduit; (a) Secondary $\mathbf{Re}$ = 100, (b) Secondary $\mathbf{Re}$ = 200, (c) Primary $\mathbf{Re}$ = 100, and (b) Primary $\mathbf{Re}$ = 200.

4.3.3 *Effect of Fluid Type*

For viscoelastic fluid, the secondary flow was studied under the identical conditions as mention earlier. In the case of straight conduit with various shaped, the simulated results shown that the secondary flow strength of circular conduit was identical with Newtonian fluid. However, the highest value was occurred in the triangular conduit as show in Table 4.8

Table 4.8 The secondary flow strength of viscoelastic fluid in various shaped conduits.

Conduit shape	The strength of secondary flow (%)
Circular	0.0249
Elliptic	0.2249
Triangular	0.2475
Square	0.1402
Hexagonal	0.0931
Octagonal	0.0654

The secondary flow strength in straight conduit given by viscoelastic fluid more corresponded to the unbalance of direct shear stress that occurred by non-axisymmetric conduit.

The two important effect of viscoelastic properties on the occurrence of secondary flow were the higher value of secondary flow strength and the orderly vortices patterns (at low Reynolds number: $\mathbf{Re}$ = 5) which two-vortices were occurred at the corners of the conduit except of circular conduits as shown in Figure 4.23 and Figure 4.24. This effect were occurred by the higher value of shear stress and the higher unbalance of shear stress in itself as shown in Figure 4.25. These higher also gave the corresponded result agree with the unbalance of direct stress that given by conduit shape as reported earlier (Figure 4.9)

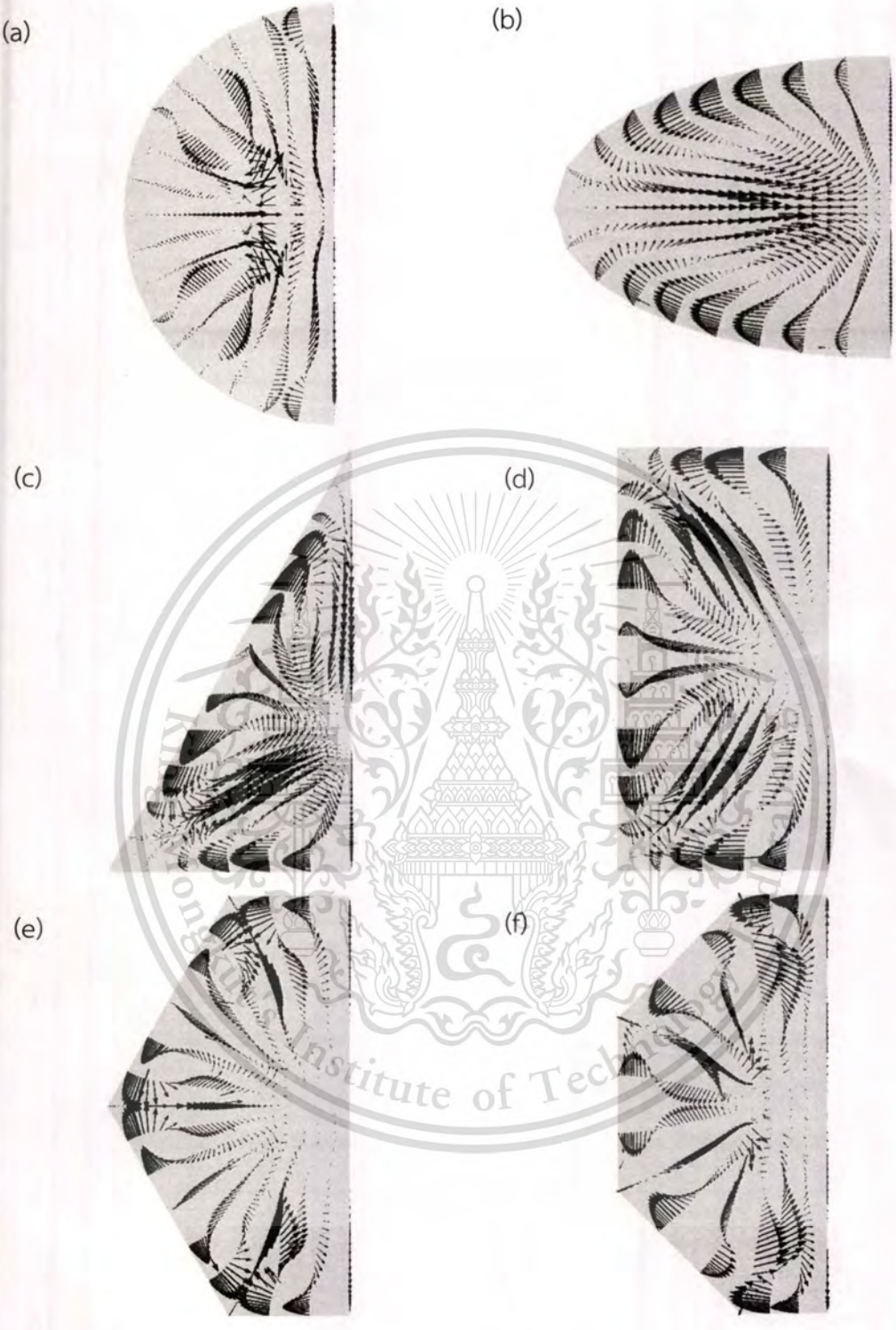

Figure 4.23 Velocity vector profile of secondary flow of viscoelastic fluid in various shaped conduit; (a) circular, (b) elliptic, (c) triangular, (d) square, (e) hexagonal, and (f) octagonal shape conduit.

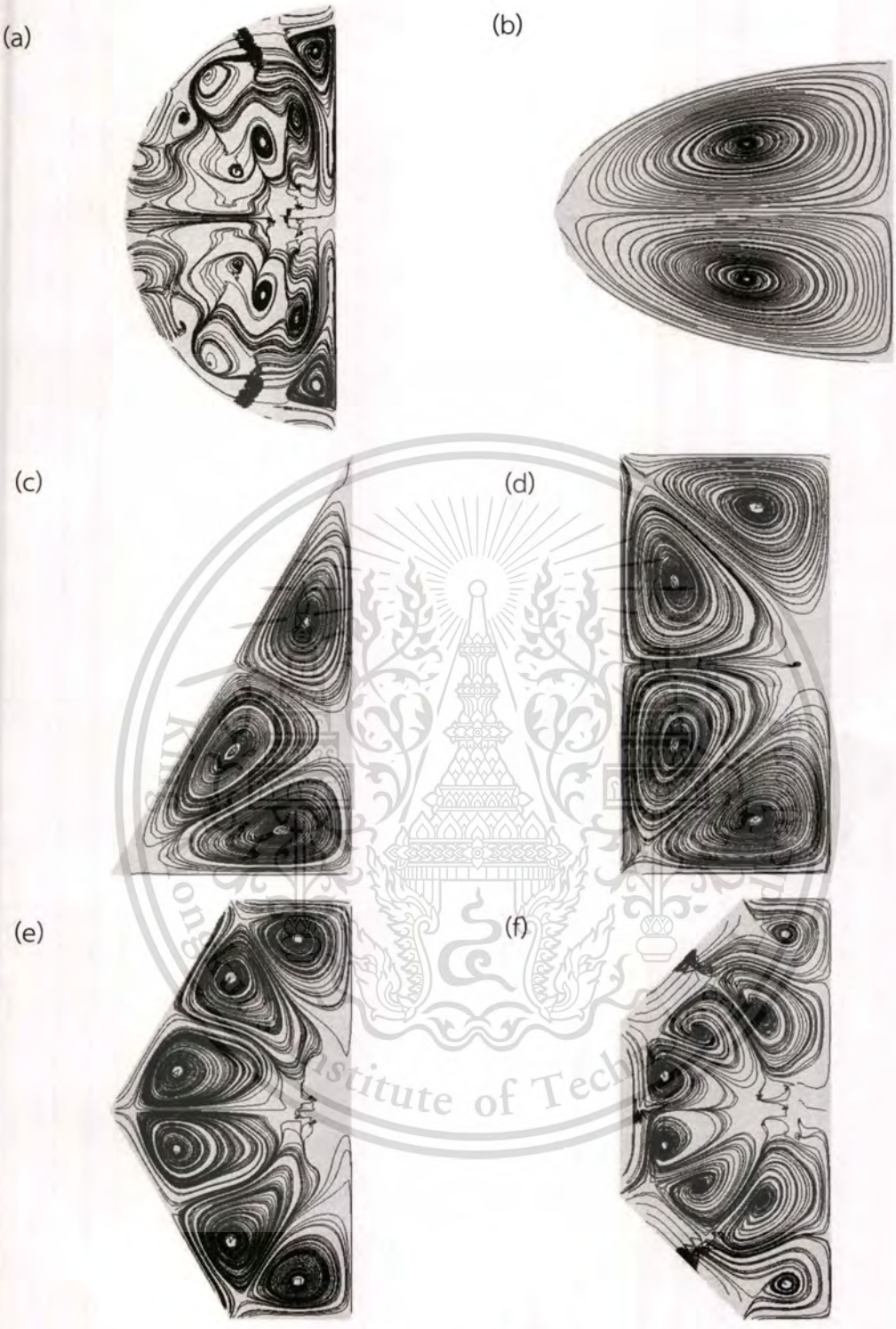

Figure 4.24 Streamline of secondary flow of viscoelastic fluid in various shaped conduit; (a) circular, (b) elliptic, (c) triangular, (d) square, (e) hexagonal, and (f) octagonal shape conduit.

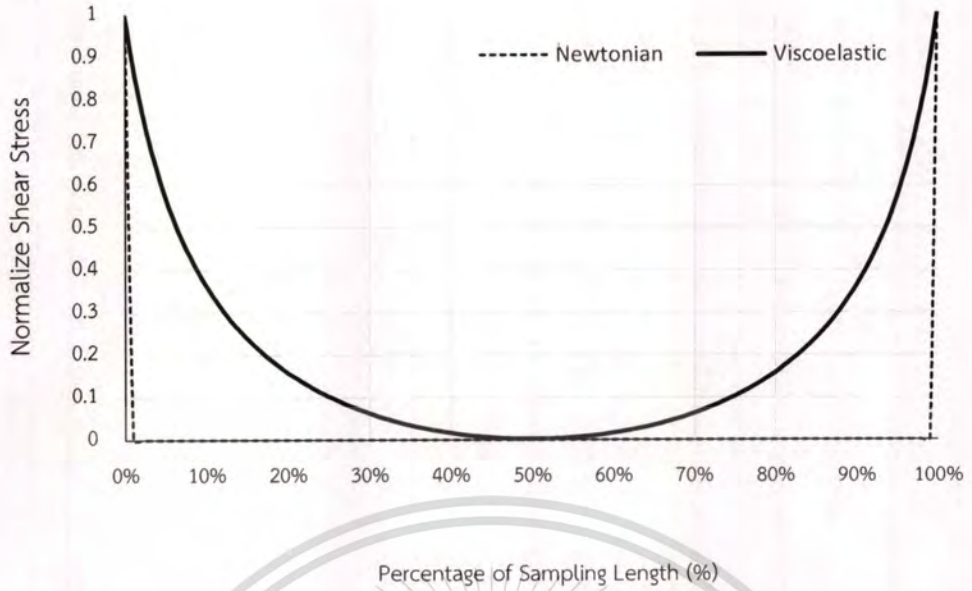

Figure 4.25 The comparison between normalize direct shear stress of Newtonian and viscoelastic fluid at the center of square conduit.

In the case of curved conduit, the appearance of secondary flow pattern in each conduit was similar to Newtonian fluid. As mention earlier, the pressure gradient affected on the unbalance of direct stresses. This unbalance was stabilized by adjusting the viscosity, which depend on shear stress, instead of the secondary flow generation.

For the effect of inlet velocity, the strength of secondary flow in straight conduit was also similar to Newtonian fluid which the secondary flow strength is proportional to the increasing of inlet velocity as displayed in Figure 4.26. However, secondary flow pattern for viscoelastic fluid when the inlet velocity was increased, was in conflict with Newtonian Fluid. The variation of cross – stream velocities were induced to the corners of the conduit instant of the center as the Newtonian fluid did and this effect, also impact on the primary flow which expand their core flow to became larger than low velocity inlet as shown in Figure 4.27.

For curved conduit case, The increasing of inlet velocity in curved conduit was observed at only $\mathbf{Re}$ = 10 because the higher inlet velocity produced more viscosity which lead to the condition that unable to simulated by this outlet boundary condition setup (zero pressure). The occurred condition required vacuum boundary condition at the outlet of the conduit to flow this fluid.

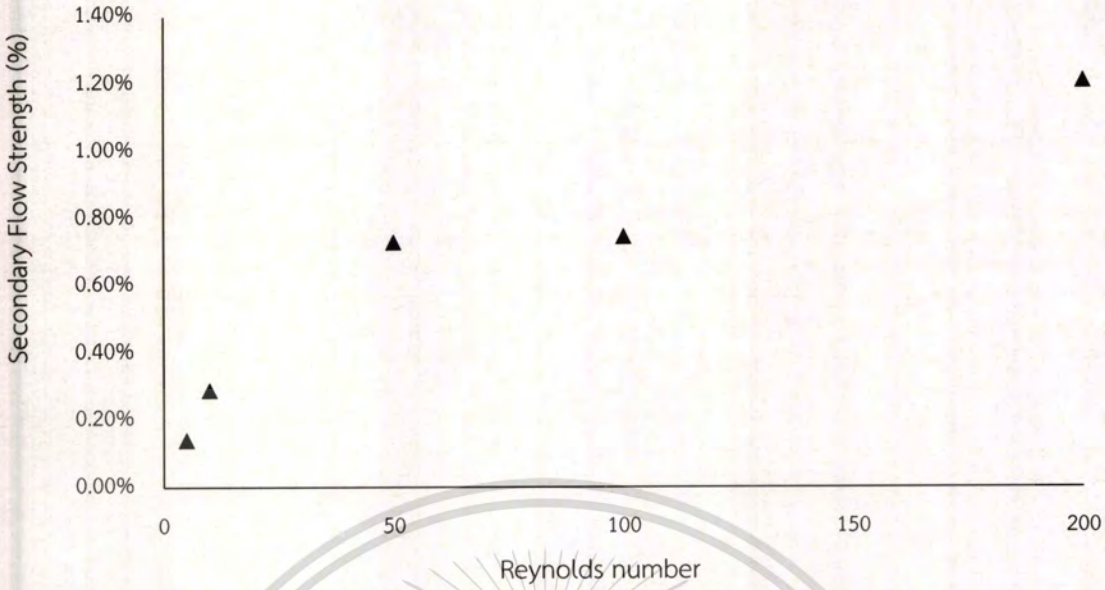

Figure 4.26 The secondary flow strength of viscoelastic fluid in straight square conduits by various Reynolds number.

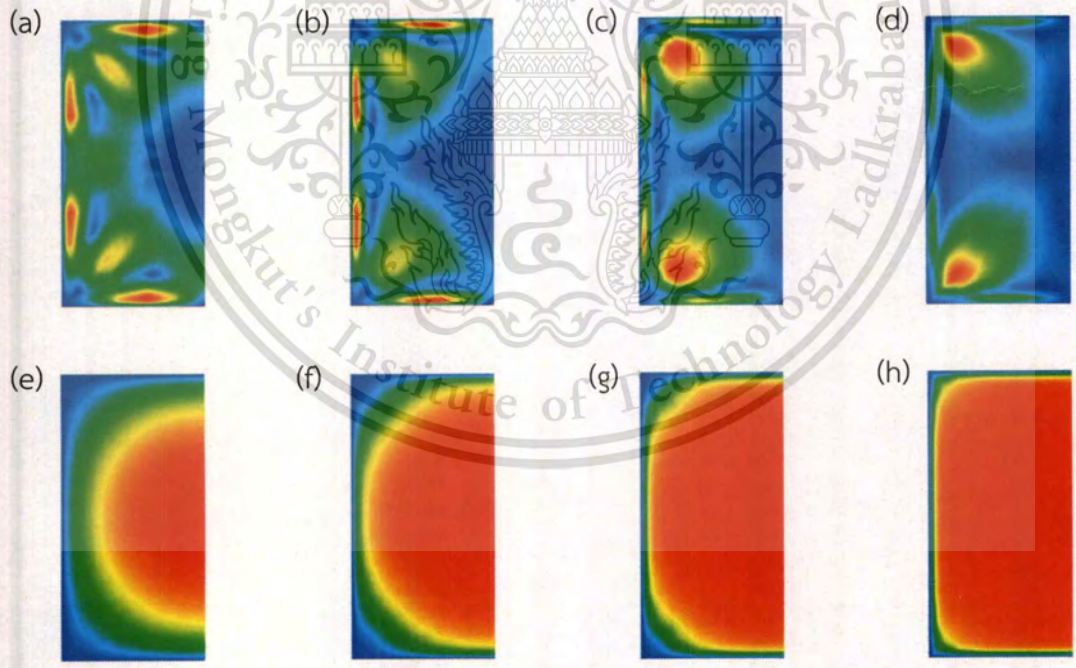

Figure 4.27 The secondary flow and primary velocity contour of viscoelastic fluid in various inlet velocities; Secondary flow (a) **Re** = 10, (b) **Re** = 50, (c) **Re** = 100, (d) **Re** = 200, Primary flow (e) **Re** = 10, (f) **Re** = 50, (g) **Re** = 100, and (h) **Re** = 200.

CHAPTER V

CONCLUSIONS AND RECOMMENDATION

5.1 Conclusions

The secondary flow in various shape conduits and flow conditions was investigated by using a CFD program, OpenFOAM®. The study focused on the appearance of secondary flows and their mechanism. The flow domains were symmetric three – Dimensional model which the symmetry boundary condition to reduce a number of mesh and computational effort in problem. Fluids were considered to be isothermal and incompressible. The fluid motion was considered to be laminar flow. The Giesekus constitutive equation was applied to simulate the flow motion of viscoelastic fluid. Mesh generation of all models was generated with mesh size of the initial mash size multiply by 1.5. The velocity profile for both fluid type were in good agreement with the theory and the previous simulated data [17].

The main contribution of this study can be concluded into three main parts:

1) Non – axisymmetric shape conduits including triangle, square, and hexagon and all of curved conduits give a higher value of secondary flows strength in both of two fluid types because of an increase of the unbalance direct stresses, especially, the unbalance from the presence of pressure gradient when conduits were bended.

2) The secondary flow strength is proportional to an increase of inlet velocity of both fluid types. For Newtonian fluid, this increase also causes the induction of cross –stream velocity to the center of the conduit. In contrast with viscoelastic fluid which causes the induction to the corner of the conduit instead.

3) Additional stress tensor in viscoelastic fluid affects transverse flow field stronger than the axial flow field.

5.2 Recommendation

1) Use full model instead of half model geometry to observe the more realistic results.

2) Use multi-mode instant of single mode of constitutive equation for viscoelastic fluid to get the better and more accurate results.

REFERENCES

[1] Xue S.-C., Phan-Thien N., Tanner R.I. **"Numerical study of secondary flows of viscoelastic fluid in straight pipes by an implicit finite volume method."** J. Non-Newtonian Fluid Mech., 59, 1995, 191-213.

[2] Letelier M. F., Siginer D.A. **"Secondary flows of viscoelastic liquids in straight tubes."** International Journal of Solids and Structures, 40, 2003, 5081–5095.

[3] Versteeg H. K., Malalasekera W. **An introduction to computational fluid dynamics the finite volume method.** Malaysia: Prentice Hall, 1995.

[4] Bakker A., Haidari A.H., Oshinowo L.M. **"Realize greater benefits from CFD. Fluid/Solids Handling."** AIChE's CEP magazine, March 2001, 45-53.

[5] Shaw C.T. **Using computational fluid dynamics.** Prentice Hall International (UK) Ltd., 1992.

[6] Eesa M. **"CFD Studies of complex fluid flows in pipes."** Ph.D. Thesis of University of Birmingham. 2009.

[7] Wilkes J.O. **Fluid Mechanics for Chemical Engineers.** Prentice Hall Professional Technical Reference, 2006.

[8] Brust M., Schaefer C., Doerr R., Pan L., Garcia M., Arratia P. E., Wagner C. **"Rheology of human blood plasma: Viscoelastic versus Newtonian behavior."** Phys. Rev. Lett., 2013.

[9] Frederickson A.G. **Principles and Applications of Rheology.** Prentice-Hall, 1964.

[10]Chan L. **"Experimental Observations and Numerical Simulation of the Weissenberg Climbing Effect."** Ph.D. dissertation, University of Michigan, Ann Arbor, 1972, 34.

[11] Geankoplis, Christie J. **Transport Processes and Separation Process Principles.** Prentice Hall Professional Technical Reference, 2003.

[12] Dubaj **"Laminar and turbulent flows."** [Online]. Available:http://commons.wikimedia.org/wiki/File:Toky.png. 2006.

[13] Reynolds A.J. **Turbulent Flows in Engineering**. Wiley, London, 1974.

[14] Yue P., Dooley J., Fenga J. J. **"A general criterion for viscoelastic secondary flow in pipes of noncircular cross section."** J. Rheol., 52(1), 2008. 315-332.

[15] Norouzia M., Kayhania M. H., Shub C., Nobaric M. R. H. **"Flow of second-order fluid in a curved duct with square cross-section."** J. Non-Newtonian Fluid Mech., 165, 323–339, 2010.

[16] Chu J.C., Teng J.-T., Xu T.-t., Huang S., Jin S., Yu X.-f., Dang T., Zhang C.-p., Greif R. **"Characterization of frictional pressure drop of liquid flow through curved rectangular microchannels."** Experimental Thermal and Fluid Science, 38, 2012, 171 – 183.

[17] Faveroa J. L., Secchib A. R., Cardozoa N. S. M., Jasakc H. **"Viscoelastic flow analysis using the software OpenFOAM and differential constitutive equations."** J. Non-Newtonian Fluid Mech., 165, 2010, 1625–1636.

[18] Azaiez J., Guénette, R., Ait-Kadi, A., **"Numerical simulation of viscoelastic flows through a planar contraction."** J. Non-Newtonian Fluid Mech. 62, 1996, 253–277.

[19] Quinzani, L.M., Armstrong R.C., Brown R.A. **J. Non-Newtonian Fluid Mech.** 52, 1994, 1–36.

[20] Stern F., Wilson R. V., Coleman H. W., Paterson E. G. **"Verification and validation of CFD simulations."** IIHR Report No. 407. Iowa: Iowa Institute of Hydraulic Research, 1999.

VITA

NAME	Mr. Tupthai Seethao
DATE OF BIRTH	August 22, 1989 in Phrae, Thailand

EDUCATIONAL RECORD

HIGH SCHOOL	High School Graduation
	Phiriyalai School Phrae, 2008
BACHELOR'S DEGREE	Bachelor of Engineering (Chemical Engineering)
	King Mongkut's Institute of Technology Ladkrabang, 2012
MASTER'S DEGREE	Master of Engineering (Chemical Engineering)
	King Mongkut's Institute of Technology Ladkrabang, 2014